INSTRUCTION REPORT S-77-1

PROCEDURES FOR DEVELOPMENT OF CBR DESIGN CURVES

by

A. Taboza Pereira

Soils and Pavements Laboratory
U. S. Army Engineer Waterways Experiment Station
P. O. Box 631, Vicksburg, Miss. 39180

June 1977
Final Report
Supersedes WES Instruction Report 4, dated November 1959

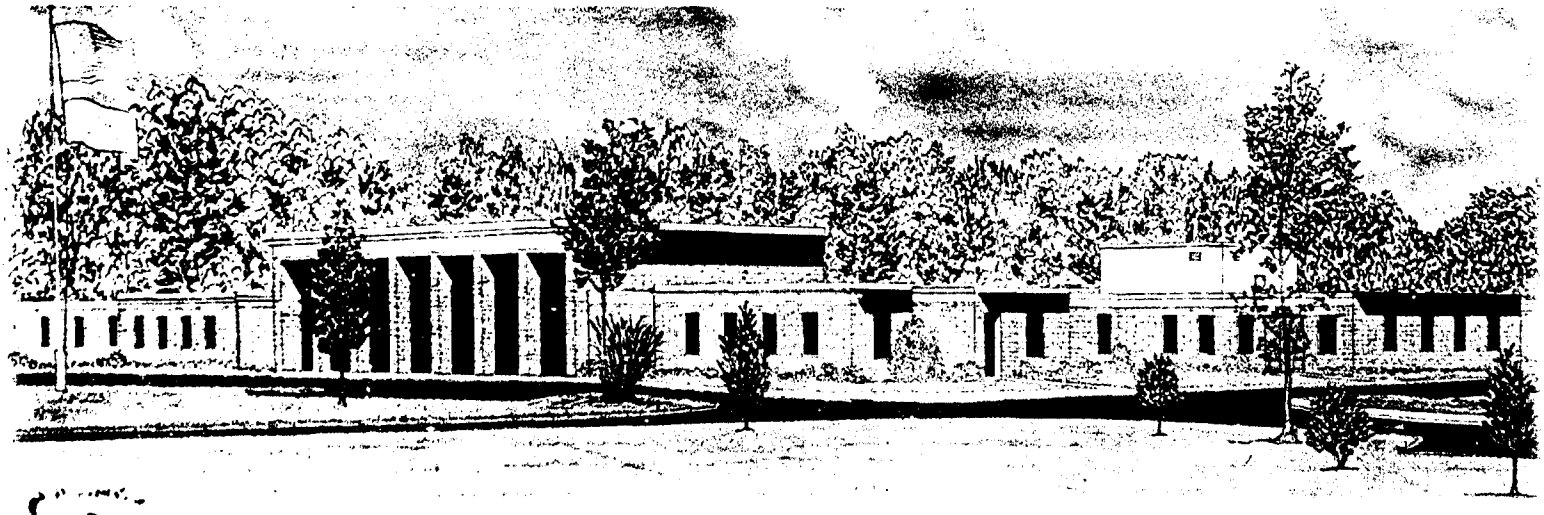

Prepared for Office, Chief of Engineers, U. S. Army
Washington, D. C. 20314

Under Project 4A762719AT40
Task A2, Work Unit 001

Destroy this report when no longer needed. Do not return it to the originator.

Unclassified
SECURITY CLASSIFICATION OF THIS PAGE (When Data Entered)

REPORT DOCUMENTATION PAGE

READ INSTRUCTIONS BEFORE COMPLETING FORM

1. REPORT NUMBER: Instruction Report S-77-1	2. GOVT ACCESSION NO.
3. RECIPIENT'S CATALOG NUMBER	
4. TITLE (and Subtitle): PROCEDURES FOR DEVELOPMENT OF CBR DESIGN CURVES.	5. TYPE OF REPORT & PERIOD COVERED: Final report.
	6. PERFORMING ORG. REPORT NUMBER: Nov 76 - Mar 77.
7. AUTHOR(s): A. Taboza Pereira	8. CONTRACT OR GRANT NUMBER(s)
9. PERFORMING ORGANIZATION NAME AND ADDRESS: U. S. Army Engineer Waterways Experiment Station, Soils and Pavements Laboratory, P. O. Box 631, Vicksburg, Miss. 39180	10. PROGRAM ELEMENT, PROJECT, TASK AREA & WORK UNIT NUMBERS: Project 4A762719AT40, Task A2, Work Unit 001
11. CONTROLLING OFFICE NAME AND ADDRESS: Office, Chief of Engineers, U. S. Army, Washington, D. C. 20314	12. REPORT DATE: June 1977
	13. NUMBER OF PAGES: 89
14. MONITORING AGENCY NAME & ADDRESS (if different from Controlling Office)	15. SECURITY CLASS. (of this report): Unclassified
	15a. DECLASSIFICATION/DOWNGRADING SCHEDULE

16. DISTRIBUTION STATEMENT (of this Report)

Approved for public release; distribution unlimited.

17. DISTRIBUTION STATEMENT (of the abstract entered in Block 20, if different from Report)

18. SUPPLEMENTARY NOTES

Supersedes WES Instruction Report 4, "Developing a Set of CBR Design Curves," November 1959.

19. KEY WORDS (Continue on reverse side if necessary and identify by block number)

California Bearing Ratio
Flexible pavements
Pavement design
Pavements

20. ABSTRACT (Continue on reverse side if necessary and identify by block number)

The pattern of design relations for flexible pavements was established and reported in WES Instruction Report 4. This pattern has been modified in recent years and new relations established. This report presents the current procedures for determining flexible pavement thickness requirements.

The CBR-thickness relationship can be portrayed by an equation or by a combined CBR curve. This report shows how, by use of equivalent single-wheel

(Continued)

DD FORM 1 JAN 73 1473 EDITION OF 1 NOV 65 IS OBSOLETE

Unclassified
SECURITY CLASSIFICATION OF THIS PAGE (When Data Entered)

20. ABSTRACT (Continued).

loads, the single-wheel design criteria can be applied to any multiple-wheel configuration. Means are also presented for developing either single-wheel or multiple-wheel design criteria for various levels of usage based on load repetitions. A detailed example demonstrating equivalent single-wheel load determinations, pass-per-coverage relationships, and thickness requirements is presented.

PREFACE

The investigation reported herein was sponsored by the Office, Chief of Engineers (OCE), U. S. Army, as a part of Project 4A762719AT40, Task A2, Work Unit 001, "Construction Design Technology Base." OCE Technical Monitor for this investigation was Mr. A. F. Muller (DAEN-MCE-D).

The investigation was conducted during the period March 1976 to March 1977 at the U. S. Army Engineer Waterways Experiment Station (WES) by personnel of the Soils and Pavements Laboratory (S&PL) under the general supervision of Messrs. J. P. Sale and R. G. Ahlvin, Chief and Assistant Chief of the S&PL, respectively. Personnel engaged in preparation of this report were MAJ A. Taboza Pereira, an exchange officer from Brazil, and Messrs. D. M. Ladd, Chief, Design Criteria Branch, and H. R. Austin, Mathematician. This report was written by MAJ Pereira.

Director of WES during the conduct of this investigation and the preparation of this report was COL J. L. Cannon, CE. Technical Director was Mr. F. R. Brown.

CONTENTS

CONVERSION FACTORS, U. S. CUSTOMARY TO METRIC (SI)
UNITS OF MEASUREMENT

U. S. customary units of measurement used in this report can be converted to metric (SI) units as follows:

Multiply	By	To Obtain
inches	25.4	millimetres
feet	0.3048	metres
square inches	6.4516	square centimetres
pounds (mass)	0.4535924	kilograms
kips (mass)	453.5924	kilograms
pounds (force) per square inch	6894.757	pascals

PROCEDURES FOR DEVELOPMENT OF CBR DESIGN CURVES

PART I: INTRODUCTION

Purpose and Scope

1. Significant changes in the procedure for developing CBR (California Bearing Ratio) design curves have occurred in the past few years. The objective of this report, therefore, is to present a description of the current Corps of Engineers (CE) methodology for construction of flexible pavement design curves. This report represents an update of U. S. Army Engineer Waterways Experiment Station (WES) Instruction Report 4, "Developing a Set of CBR Design Curves," dated November 1959.[1] Procedures for computation of pass-per-coverage ratio by statistical methods are described. Also, procedures and tables for computation of deflections and equivalent single-wheel loads (ESWL) for any value of Poisson's ratio are presented, although the CE uses 0.5 for all calculations. This report was prepared to familiarize engineers with the theories and techniques for the construction of flexible pavement design curves.

Background

2. The CBR method has been used since the early 1940's in airfield pavement design.[1-4] This method has been improved repeatedly as the result of continuous research and field observations through the years. The method may be considered semiempirical, since it was developed using concepts and mathematical developments of the elastic theory, together with data taken from test sections and airfields under prototype aircraft traffic.

3. In computing pavement thickness through the CBR design method, the following data must be known: volume of traffic, load, type of design aircraft, and soil strength. These parameters account for the

magnitude and distribution of load, as well as the frequency with which the pavement and the subgrade have to undergo stresses. The soil strength, represented by the CBR, indicates the ability of a soil to withstand wheel loads. CBR is not a direct measurement of the soil bearing capacity, but is an index of the soil strength determined by comparison with a standard value.

4. The CBR design method for flexible pavements was conceived initially by the California Highway Department to compute pavement thickness for single-wheel loads on highways. The method was then adapted by the CE for airfield design. Following the development of larger aircraft, the method was adapted for multiple-wheel loads[5,4] by studying the effect of uniform circular loads acting on a homogeneous, isotropic, and elastic half space, through use of the classical Boussinesq theory.

5. Results of extensive tests on full-scale test sections trafficked with multiple-wheel heavy gear loads, in conjunction with statistical studies of the traffic behavior on airfields, have recently led to important improvements in this design method. A new procedure was developed to deal with the effect of lateral distribution of traffic on runways and taxiways, and consequently an improved method was found to relate the number of operations of an aircraft to the number of design stress applications to the pavement (passes per coverage ratio). Also, the effect of multiple wheels on pavements was restudied and a relationship was established between the number of wheels on the main assembly and the effect of stress repetitions (load repetitions factor) on thickness. The overall result of these developments on pavement design was to reduce the required flexible pavement thicknesses for a given loading condition.

PART II: TRAFFIC STUDY

General

6. Traffic is one of the primary parameters affecting airfield pavement design. Airfields are usually designed for a given number of passes of a specific aircraft having definite characteristics. The number of passes of the design aircraft is directly related to the number of times the pavement is subjected to the maximum stress and, consequently, defines the pavement life. In this part of the report, the relationship between the number of passes of the design aircraft and the number of stress applications to the pavement will be mathematically defined, and the manner in which this relationship affects the pavement design will be discussed.

Lateral Distribution of Traffic

Theoretical considerations

7. Usually, runway and taxiway center lines are marked as a reference for pilots. As a consequence, the traffic tends to be channelized, with the highest concentration in the vicinity of the center lines. Theoretically, the probability of running on the right or left side of the geometric center line in any single use of the airfield facility is fifty percent for each side. Therefore, for a small number of passes, the traffic may be considered to follow the pattern of a binomial distribution or discrete probability distribution,* and tends to the normal or Gaussian distribution as the traffic increases. (*Note: The binomial distribution, also called Bernoulli distribution or discrete probability distribution, is given by the expressions

$$p(x) = {}_{N}C_{x} p^{x} q^{(N-x)}$$

and

$$ {}_{N}C_{x} = \frac{N!}{x!(N-x)!} $$

where

x = the number of times an event will probably happen in N trials

p = the probability that an event will happen in any single trial

q = the probability that an event will fail to happen in any single trial

Example: In 6 takeoffs, the probability that an aircraft will run 2 times on the left side of a runway center line is

$$ p(2) = {}_{6}C_{2}\left(\frac{1}{2}\right)^{2}\left(\frac{1}{2}\right)^{6-2} = \frac{6!}{2!4!} \times \left(\frac{1}{2}\right)^{6} = 0.23 $$

As the number of trials increases, and if p or q is not close to zero, the discrete probability distribution approaches the normal distribution and, in the limiting case, when N tends to infinity, the approximation is exact.[7])

8. Since airfields are designed to sustain a very large number of passes, the traffic may be considered laterally distributed in the shape of a normal curve. Actual traffic data, taken from observations at several military airfields, show agreement with this theory.[6] Figure 1 presents a comparison between theoretical and actual distribution curves based on observations of the behavior of aircraft at three Air Force bases.

General normal distribution and standard normal distribution curves

9. According to References 7 and 8, the general normal distribution (GND) curve or Gaussian curve is defined by the equation:

$$ f(x) = \frac{1}{\sigma_x \sqrt{2\pi}} e^{-\frac{1}{2}\left(\frac{x-\mu}{\sigma_x}\right)^2} \qquad (1) $$

where x is a variable with a continuous set of values, σ_x is the standard deviation of x, μ is the mean of the x values, and f(x) is the frequency with which the x events can happen.

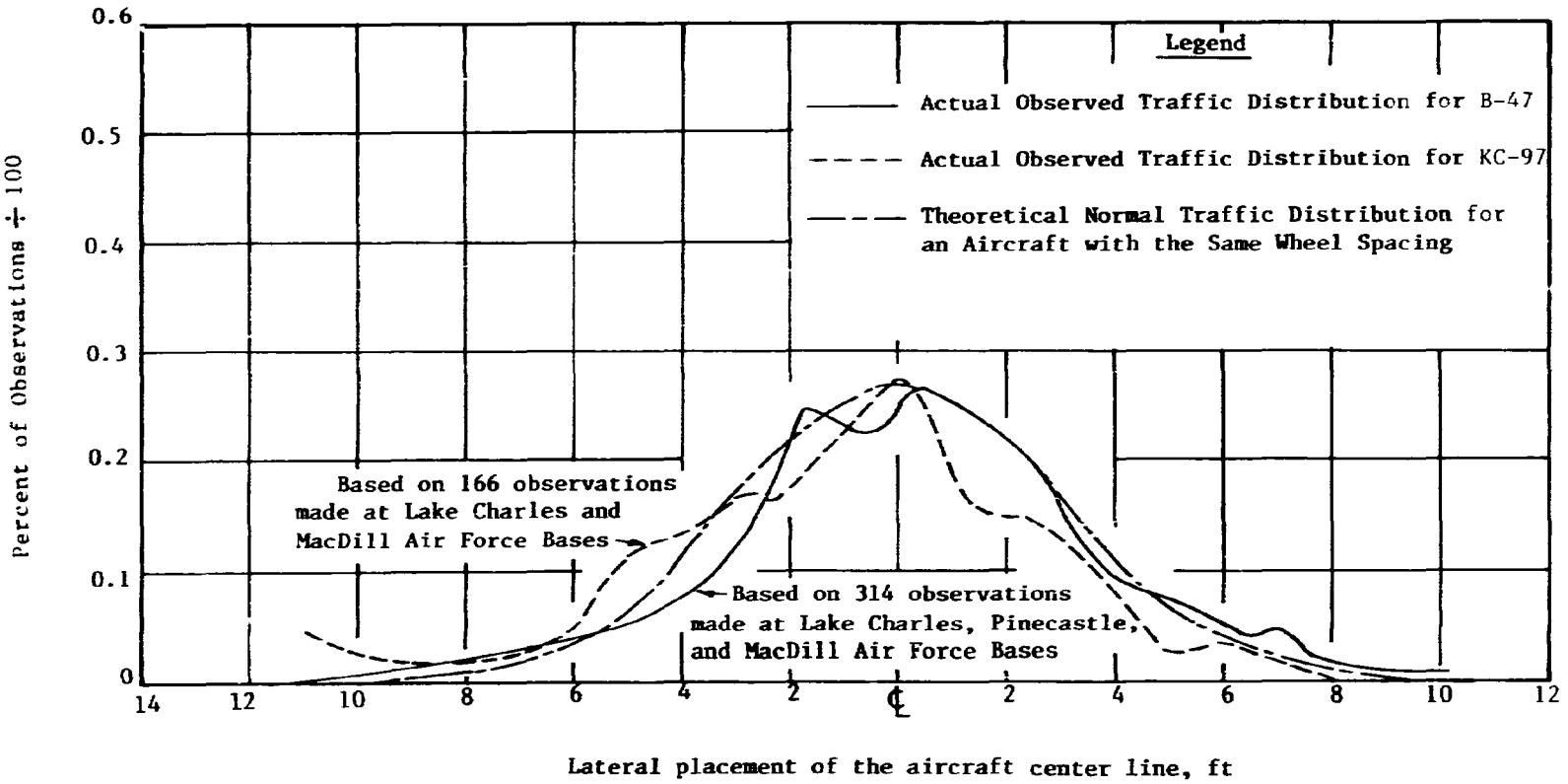

Figure 1. Distribution of B-47 and KC-97 aircraft traffic along straightways of taxiway (from Reference 6)

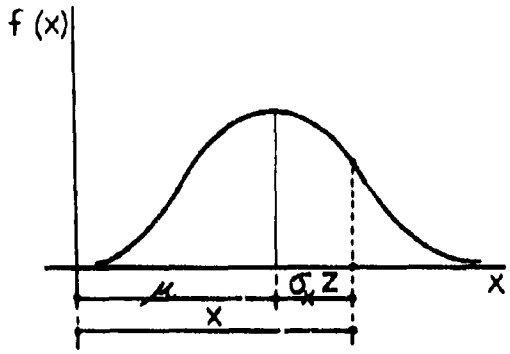

Figure 2. General normal distribution (GND) curve

10. If the deviations from the mean are measured in units of standard deviations (see Figure 2), this relationship can be expressed by

$$z = \frac{x - \mu}{\sigma_x} \tag{2}$$

and Equation 1 is replaced by the expression

$$f(x) = \frac{1}{\sigma_x \sqrt{2\pi}} e^{-\frac{1}{2} z^2} \tag{3}$$

or simply by

$$f(x) = \frac{1}{\sigma_x} f(z) \tag{4}$$

The equation of $f(z)$ is

$$f(z) = \frac{1}{\sigma_z \sqrt{2\pi}} e^{-\frac{1}{2} z^2} \tag{5}$$

But the values of z are measured in units of standard deviations; therefore, σ_z equals one, and Equation 5 may be written as follows:

$$f(z) = \frac{1}{\sqrt{2\pi}} e^{-\frac{1}{2} z^2} \qquad (6)$$

In this case, z is called a standardized variable and is a dimensionless quantity. The deviations from the mean are said to be expressed in standard units; the standard deviation equals one and the mean equals zero. Equation 6 represents the standard normal distribution (SND) curve as illustrated in Figure 3.

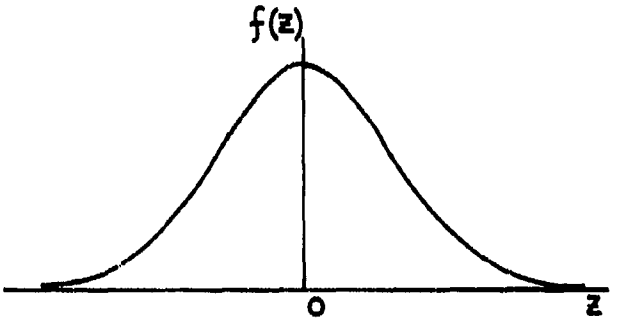

Figure 3. Standard normal distribution (SND) curve

Some properties of the SND curve are tabulated in statistics books.[7,8] For example: (a) For z equal to zero, the maximum ordinate [$f(z)$] equals 0.3989. For z equal to 3.99, $f(z)$ equals 0.0001. The minimum ordinate corresponds to the limiting case, when z tends to infinity. (b) For z equal to zero, the area under the curve equals zero. For z equal to 3.99, the area under the curve equals 0.5000.

11. Ordinates and areas under the curve can be taken from tables for any value of z, from 0.00 to 3.99. Due to the symmetry of the SND curve, the ordinate values are the same for the corresponding negative abscissas.

12. The data in Table 1 for the SND curve can be used in the application of the normal curve to the aircraft traffic study.

Application of the GND and SND curves to aircraft traffic

13. The distribution of aircraft traffic on runways and taxiways

may be represented by a GND curve, where the ordinate represents the frequency of the passes of the aircraft center line at a certain distance from the pavement center line. This distance from the center line is plotted as the abscissa using conventional methods.

14. Obviously, the same curve also represents the transverse variation in the placement of the aircraft tires on the pavement. This concept permits the presentation of two important definitions: wander and coverage.

a. Wander is defined in Reference 6 as "the width over which the center line of aircraft traffic is distributed 75 percent of the time." Based on previous considerations, the same concept may be extended to the center line of one tire. Currently, a wander width of 70 in.* is used for taxiways and the first 1000 ft of each runway end. A wander width of 140 in. is used for the runway interior. These values are based on actual traffic observations.[6]

b. Coverage is defined as the application of the maximum stress on a point in a pavement surface. Therefore, when a pavement is designed for a particular wheel load, one coverage is being applied to a point on the pavement each time this wheel load passes over that point. To illustrate this concept with an example, assume a pavement will be subjected to the traffic of a single-wheel load with tire width W_t. This pavement is divided transversely in strips, so that one tire pass on a strip corresponds to one coverage on that strip. Assume the traffic is applied according to the pattern shown in Figure 4, so that in 100 passes the tire runs on the center strip 16 times. In this situation, it can be said that 16 coverages have been applied to the pavement and the ratio between the number of coverages and the total number of passes is

$$\frac{C}{P} = \frac{16}{100} = 0.16$$

or

$$C = 0.16P$$

---

* A table of factors for converting U. S. customary units of measurement to metric (SI) units is presented on page 3.

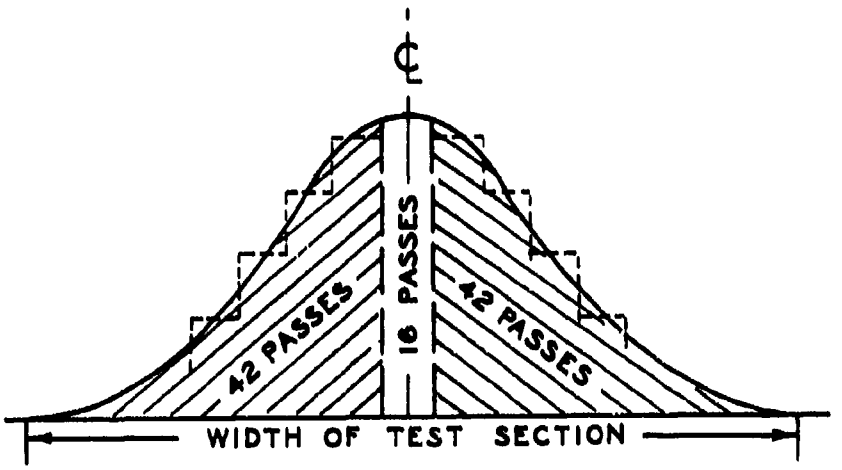

Figure 4. Example of traffic distribution in test section

Based on this example, it can be concluded that every time one tire passes on a strip, one coverage is being applied to that strip, and the number of coverages on the pavement computed for design purposes would be the number of coverages applied to that strip where the maximum accumulation occurs.

15. Now, assume that Figure 5 represents the traffic distribution on a taxiway. The ordinates, $f(x)$, represent the frequency of the passes at a point x, or the ratio between the number of passes $p(x)$ of a tire center line at a point and the total number of passes P on the taxiway. Then

$$f(x) = \frac{p(x)}{P} \tag{7}$$

or

$$p(x) = f(x) \times P \tag{8}$$

If $f(x)$ is replaced by its value in Equation 4,

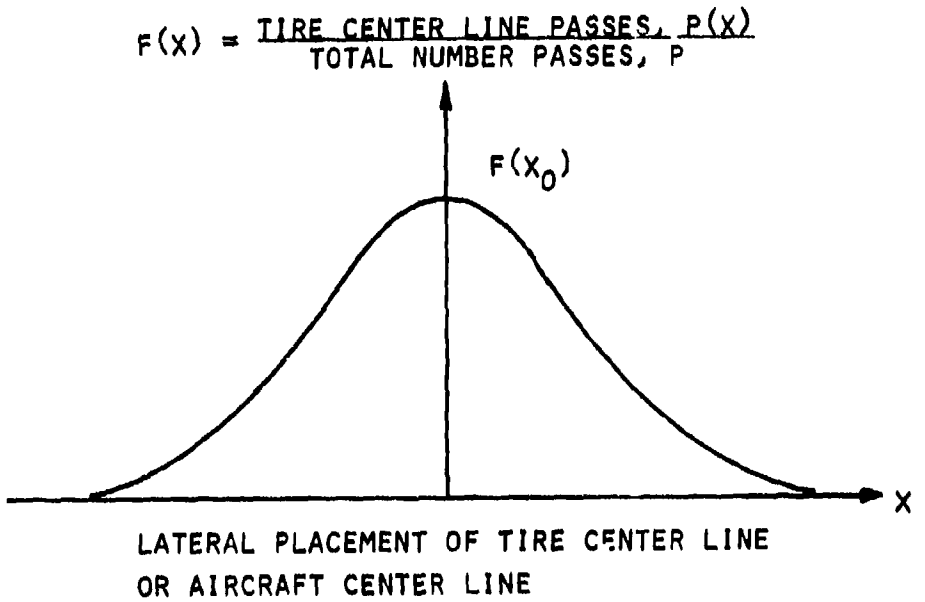

Figure 5. Theoretical normal distribution of aircraft traffic on taxiway

$$p(x) = \frac{1}{\sigma_x} f(z)P \tag{9}$$

16. The value of $p(x)$ is given in passes per measurement unit. If the value of x is measured in inches, σ_x will be in inches and $p(x)$ will correspond to passes per inch.

17. Now, a new curve can be drawn (Figure 6) with the same shape as the curve in Figure 5 where the ordinates represent the number of passes per inch of the tire center line at a particular distance from the mean value. Therefore, at a distance equal to zero, the number of passes is represented by

$$p(x_o) = f(x_o)P \tag{10}$$

or

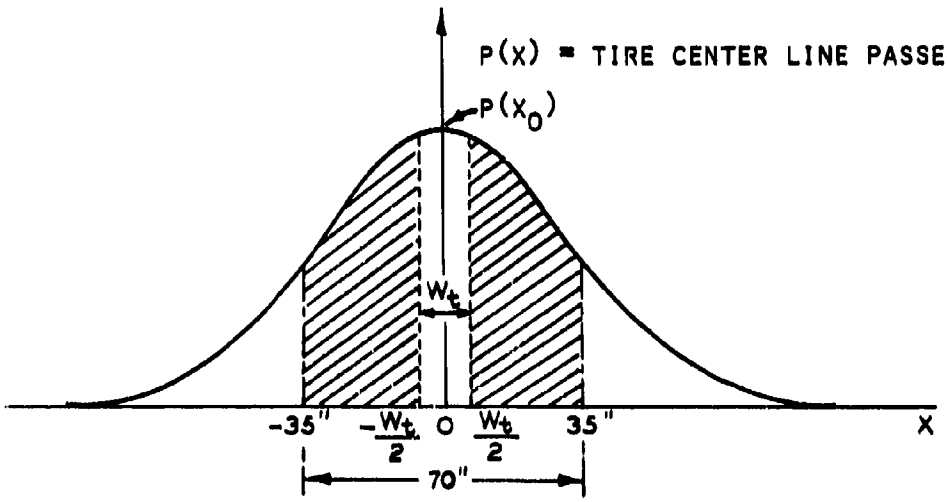

LATERAL PLACEMENT OF AIRCRAFT CENTER LINE OR TIRE CENTER LINE

Figure 6. Traffic distribution in passes per measurement unit

$$p(x_o) = \frac{1}{\sigma_x} f(z_o)P \tag{11}$$

18. If the tire width is W_t (Figure 6), then the tire applies coverages on the point $x = 0$ at every position of its own center line within the interval

$$-\frac{W_t}{2} \leq x \leq \frac{W_t}{2}$$

So, the number of coverages applied by one tire on the point $x = 0$ is given by the expression

$$C = \int_{-W_t/2}^{W_t/2} p(x)dx \tag{12}$$

or simply

$$C = p(x_o)W_t \tag{13}$$

Replacing $p(x_o)$ by its value in Equations 10 and 11, then

$$C = f(x_o)PW_t \tag{14}$$

and

$$C = \frac{1}{\sigma_x} f(z_o)PW_t \tag{15}$$

where C is the number of coverages applied by one tire, $f(z_o)$ is the maximum ordinate of the SND curve, W_t is the tire width, and P is the total number of tire passes. The computation of σ_x may be done by use of Equation 2, as follows:

$$z = \frac{x - \mu}{\sigma_x} \quad \text{or} \quad \sigma_x = \frac{x - \mu}{z}$$

By definition, for a wander width of 70 in., 75 percent of the passes (or 75 percent of the GND curve area) lie in the interval between $x = -35$ in. and $x = 35$ in. (see Figure 6). From Table 1, 75 percent of the SND curve lies in the interval between $z = -1.15$ and $z = 1.15$ (see Figure 7), and the maximum ordinate for $z = 0$ is $f(z_o) = 0.3989$. So for this particular situation,

$$\mu = 0 , \quad x = 35 , \text{ and } z = 1.15$$

and finally

$$\sigma_x = \frac{35 - 0}{1.15} = 30.43 \text{ in.} \tag{16}$$

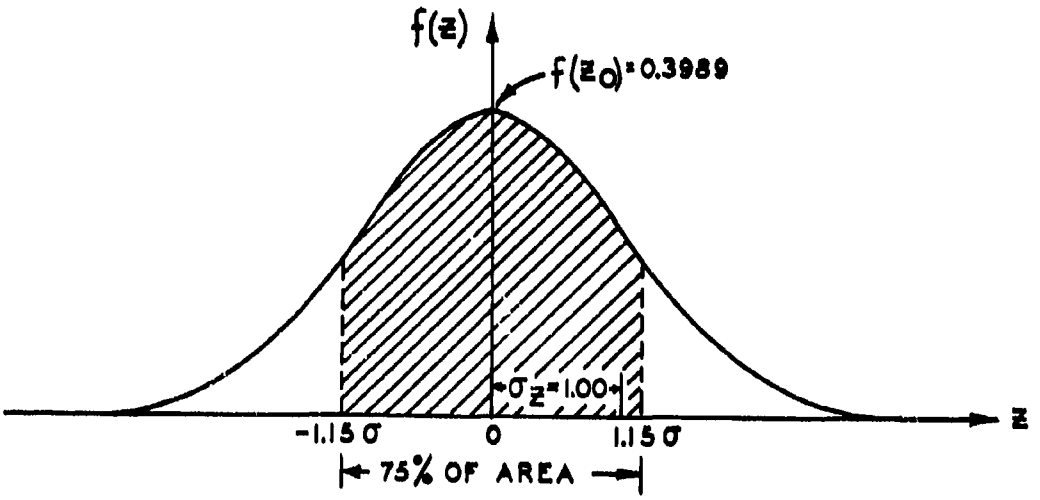

Figure 7. SND curve, as related to aircraft traffic distribution

19. For a wander width of 140 in., 75 percent of the GND curve lies between the values $x = -70$ and $x = 70$ in. Computing through the same procedure, the σ_x value will be:

$$\sigma_x = \frac{70 - 0}{1.15} = 60.87 \text{ in.} \tag{17}$$

Pass-per-coverage ratio for single-wheel aircraft

20. When the tread* on a single-wheel aircraft is large, the GND curve of one tire does not influence the GND curve of the other (Figure 8), and the maximum ordinate $p(x_o)$ for the aircraft as a whole is the same as that for one wheel. According to Reference 6, this happens when the tread equals 100 in. or more for a wander equal to 70 in., or when the tread equals 200 in. or more for a wander equal to 140 in. In this case, the computation of the number of coverages C

* Distance between the center lines of the main gears.

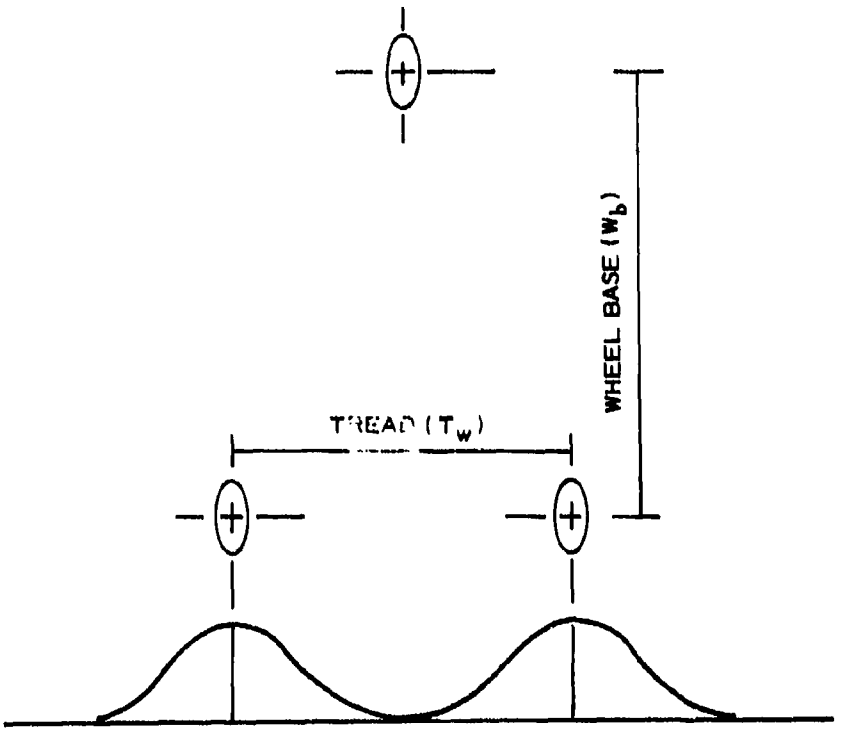

Figure 8. Typical GND curve for nonoverlapping tire prints

applied by a given number of passes P of a single-wheel aircraft on an airfield facility can be accomplished by use of Equation 15 for any value of wander.

21. The number of coverages is computed as follows for the two values of wander usually considered in airfield pavement design. For a wander of 70 in., σ_x = 30.43 in. and the number of coverages is

$$C = \frac{0.3989}{30.43} W_t P = 0.0131 W_t P^* \qquad (18)$$

---

* When W_t is not known, the following equation may be used:

$$W_t = 0.878\sqrt{\text{Tire contact area}}$$

For a wander of 140 in., σ_x = 60.87 in. and the number of coverages is

$$C = \frac{0.3989}{60.87} W_t P = 0.0065\ W_t P \tag{19}$$

The pass-per-coverage ratio can also be obtained from Equations 18 and 19. For a wander of 70 in., the ratio is

$$\frac{P}{C} = \frac{1}{0.0131\ W_t} = \frac{76.34}{W_t} \tag{20}$$

For a wander of 140 in., the ratio is

$$\frac{P}{C} = \frac{1}{0.0065\ W_t} = \frac{153.84}{W_t} \tag{21}$$

22. Single-wheel aircraft whose tread is smaller than the values presented in paragraph 20 must be treated in the same manner as for a multiple-wheel gear.

Pass-per-coverage ratio for multiple-wheel gear aircraft

23. In computing the number of coverages applied by passes of a multiple-wheel aircraft on an airfield facility, all the wheels on the main gears, as well as their arrangements, must be considered. Usually there is overlap among the GND curves of the several tires in the same assembly.

24. Figure 9 shows an example of a GND curve for overlapping tire prints of a twin-wheel aircraft. The solid lines represent the individual GND curves and the dashed lines represent the combined effect of two wheels. When the tread is small, the effects of two gears could influence each other.

25. In studying the combined effect of the wheels on a multiple-wheel gear aircraft, the individual curves can be drawn and the ordinates added graphically in the overlapping areas, and the maximum ordinate of the cumulative curve obtained.

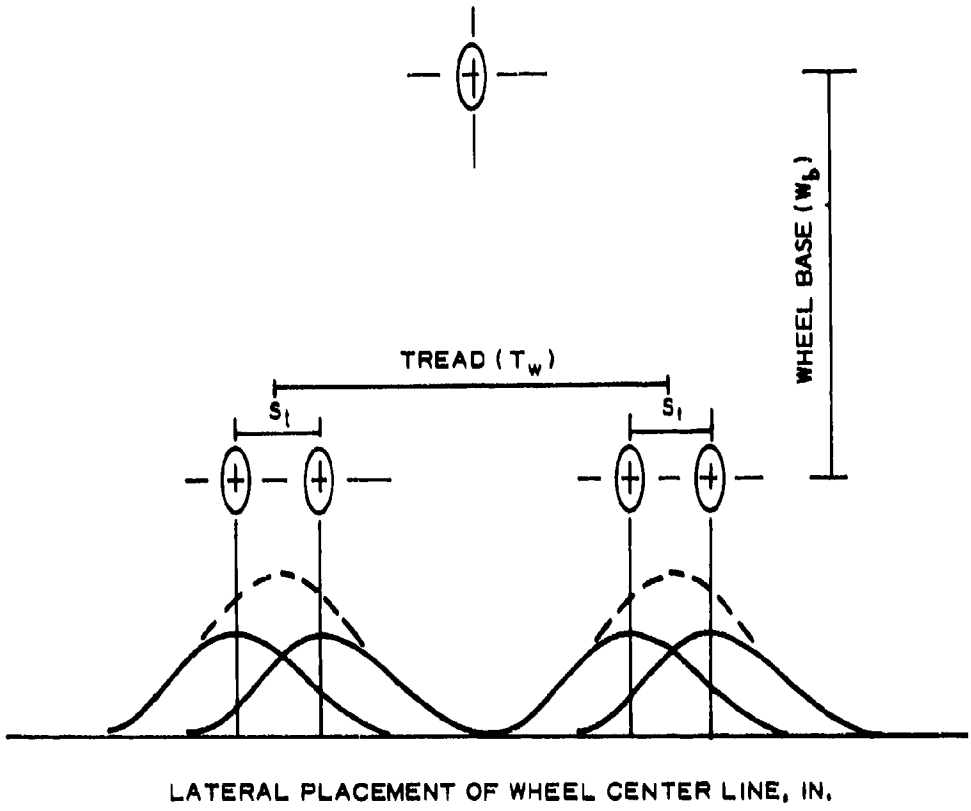

Figure 9. GND curve for overlapping tire prints, twin wheels

26. As a practical rule, for multiple-wheel gears and a wander of 70 in., the assemblies will not overlap each other when the distance between the center lines of the inside wheels (tread minus twin-wheel spacing, for the case of twin gears) is equal to 100 in. or more. When the wander width is 140 in., no overlapping of the gear is considered if the distance between the center line of the inside wheels of a multiple-wheel gear is 200 in. or more.[6]

27. For tandem wheels which track each other, the maximum ordinate of the cumulative curve equals two times the maximum ordinate of an individual curve, or $f(x_{oc}) = 2f(x_o)$.

28. The maximum ordinate of the cumulative curve $f(x_{oc})$ for any two wheels may be obtained from Figure 10. Wheel arrangements that do not follow the pattern of single, twin, and twin-tandem must have the maximum ordinates of their cumulative curves determined from their combined distribution curves.

29. Figure 11 shows the wheel configurations for typical aircraft landing gears.

30. The computation of the number of coverages C applied by a given number of passes of a multiple-wheel aircraft on a pavement can be made by use of Equation 14 for any value of wander by replacing $f(x_o)$ by the value $f(x_{oc})$ taken from the cumulative curve. So,

$$C = f(x_{oc})PW_t \tag{22}$$

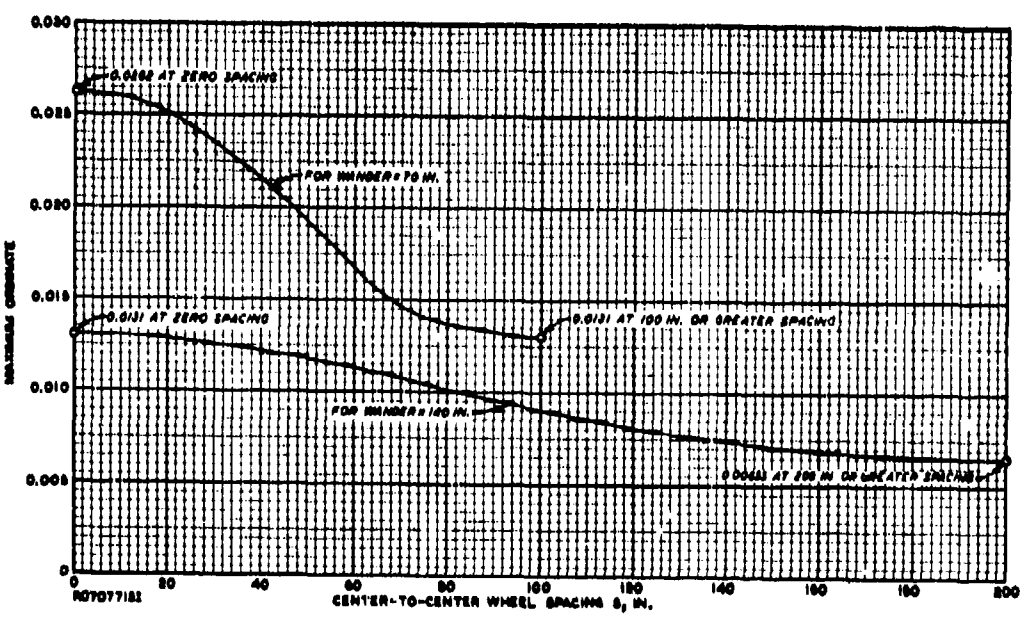

Figure 10. Maximum ordinate on cumulative traffic distribution curve for two wheels versus wheel spacing, for wander of 70 in. and 140 in. (from Reference 6)

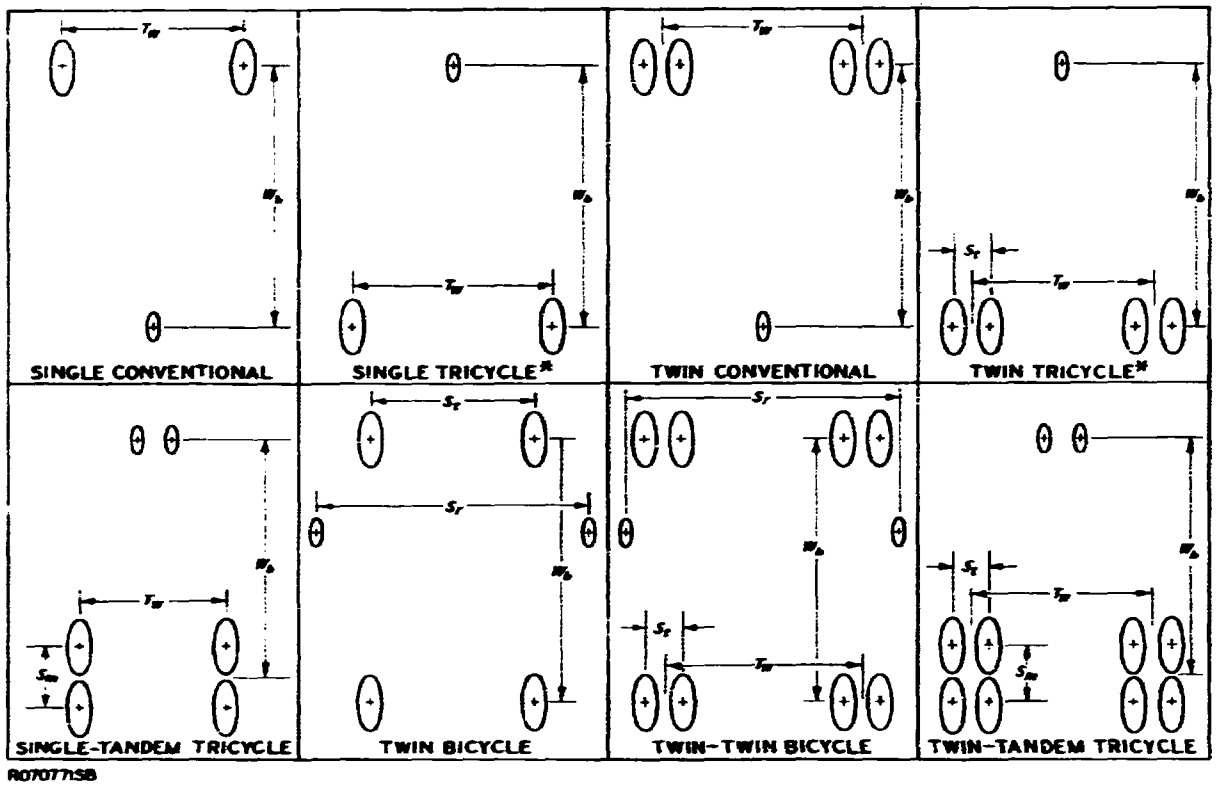

LEGEND

- T_w TREAD
- W_b WHEEL BASE
- S_t TWIN WHEEL SPACING
- S_{tm} TANDEM WHEEL SPACING
- S_r OUTRIGGER WHEEL SPACING

* THE NOSE GEAR ON SOME AIRCRAFT WITH THESE TYPES OF LANDING GEARS CONSISTS OF TWIN WHEELS.

Figure 11. Wheel configurations for typical aircraft landing gears (from Reference 6)

31. The individual curves that yield the cumulative curve are computed by relating them to the SND curve through Equation 4. The pass-per-coverage ratio is then given by the expression:

$$\frac{P}{C} = \frac{1}{f(x_{oc})\ W_t} \tag{23}$$

Practical example of pass-per-coverage ratio computation

32. Compute the pass-per-coverage ratio for the Boeing 707-100 aircraft on a taxiway. Aircraft data[6] are as follows:

Wheel arrangement: twin-tandem tricycle

Tire width (W_t) = 13.5 in.

Tread (T_W) = 265.0 in.

Twin-wheel spacing (S_t) = 34.0 in.

Tandem-wheel spacing = 56.0 in.

33. On a taxiway, the wander width is 70 in. The pass-per-coverage ratio is given by Equation 23 as follows:

$$\frac{P}{C} = \frac{1}{f(x_{oc})\ W_t}$$

The ordinates of a GND curve for one wheel are given by Equation 4:

$$f(x) = \frac{1}{\sigma_x} f(z)$$

where σ_x = 30.43 in. (for a wander of 70 in.) and $f(z)$ may be taken from Table 1. Taking several values of z, the computations may be done as in the following tabulation, for construction of the GND curve shown in Figure 12.

z	$f(z)$	$x = \sigma_x z$, in.	$f(x)$
0.00	0.3989	0.0	0.0131
0.20	0.3910	6.1	0.0128
0.50	0.3521	15.2	0.0116
1.00	0.2420	30.4	0.0080
1.50	0.1295	45.6	0.0042
2.00	0.0540	60.9	0.0018

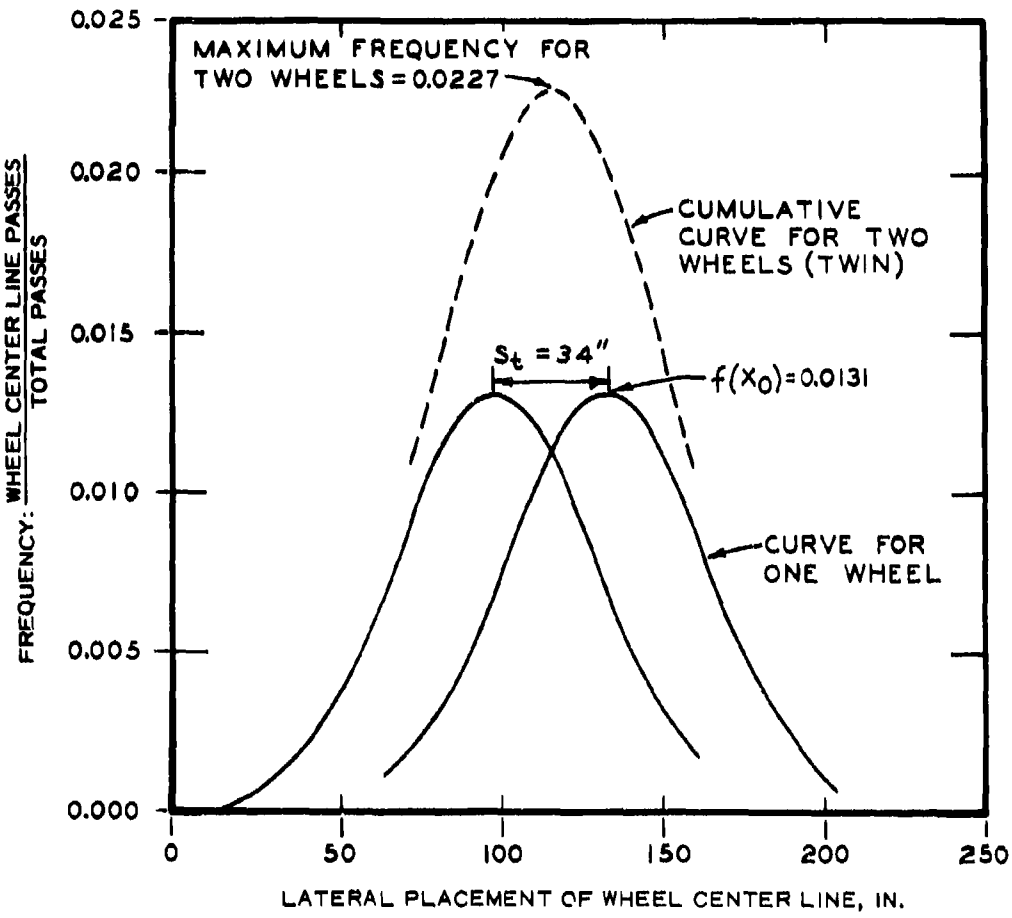

Figure 12. GND curve for the Boeing 707-100

The solid lines in Figure 12 represent the GND curves for individual wheels and the dashed line represents the cumulative curve for the front or rear twin wheels. So, the $f(x_{oc})$ value for one gear is $2 \times 0.0227 = 0.0454$. Since the wander is 70 in. and the distance between the center lines of the inside wheels $(T_W - S_t)$ is greater than 100 in., the cumulative curves of the two twin-tandem gears do not overlap. Therefore, the maximum ordinate for the Boeing 707-100 is the same as for one gear. The value of the maximum ordinate of the Boeing 707-100 GND curve could also be taken from Figure 10. Using the maximum ordinate

as determined above, the pass-per-coverage ratio can be computed using Equation 23.

$$\frac{P}{C} = \frac{1}{0.0454 \times 13.5} = 1.63$$

Effect of Load Repetitions

34. The design thickness of a pavement layer can be represented by the expression

$$t = \alpha T \tag{24}$$

where T is a standard thickness for a particular aircraft and α is a factor that adjusts the thickness according to the number of operations or repetitions of that aircraft anticipated during the pavement life. The number of operations or passes is converted to coverages through the procedure previously discussed.

35. In the past, the load repetitions factor, α, was considered to depend only upon the number of coverages (C) and was expressed as

$$\alpha = 0.23 \log C + 0.15 \tag{25}$$

This factor could be represented by a straight line on a semilog plot[1] (as shown in Figure 13). In the above equation, if C equals 5000 coverages, the α value equals one. So, according to that procedure, for 5000 coverages the design thickness is equal to the standard thickness for a particular aircraft regardless of the type of landing gear assembly.

36. Recently, extensive experiments conducted at WES determined the load repetitions factor to be dependent on the number of coverages and the number of wheels on the main landing gear assemblies.[9,10] The curves plotted in Figure 14, based on results obtained in full-scale

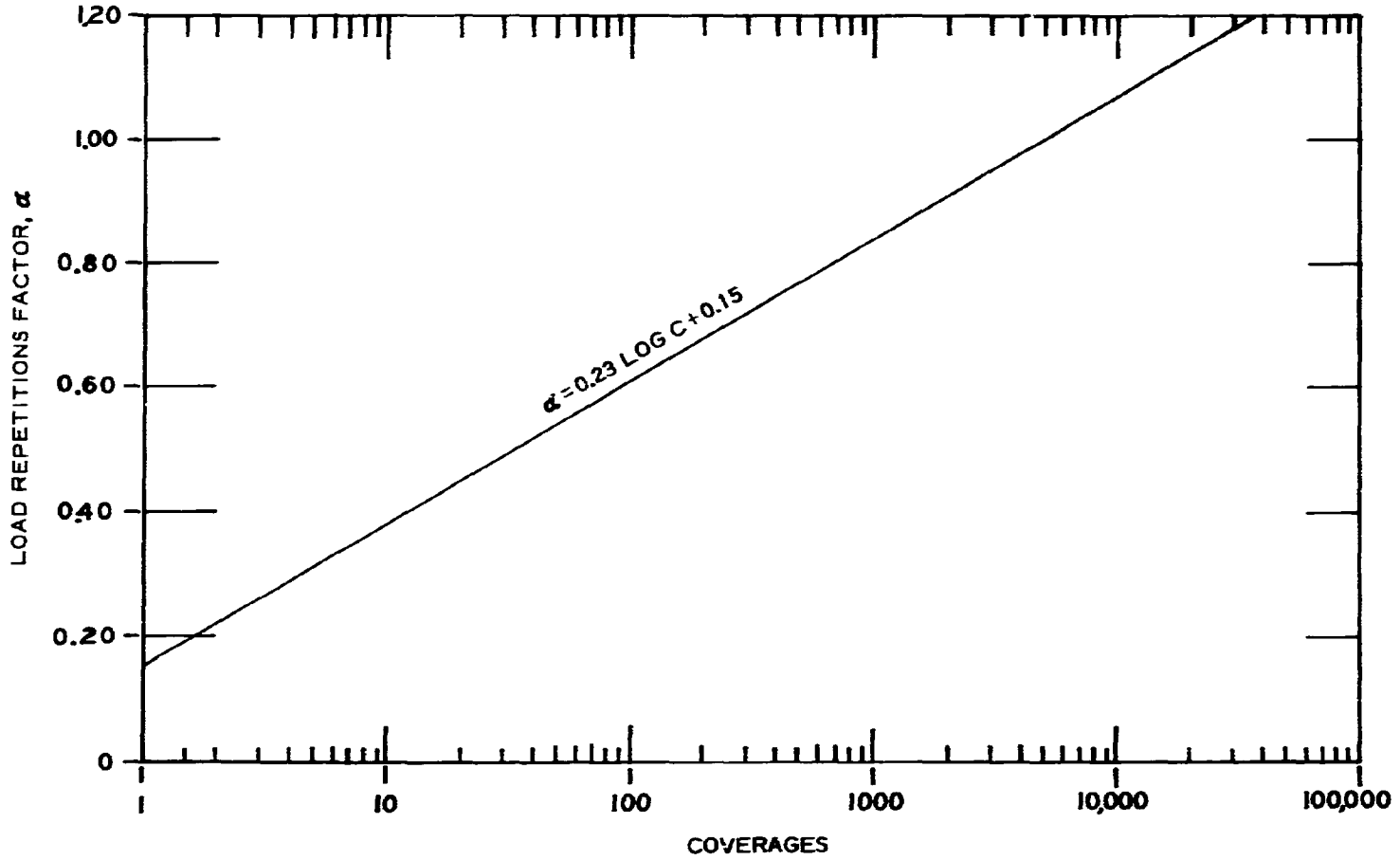

Figure 13. Load repetitions factor versus coverages

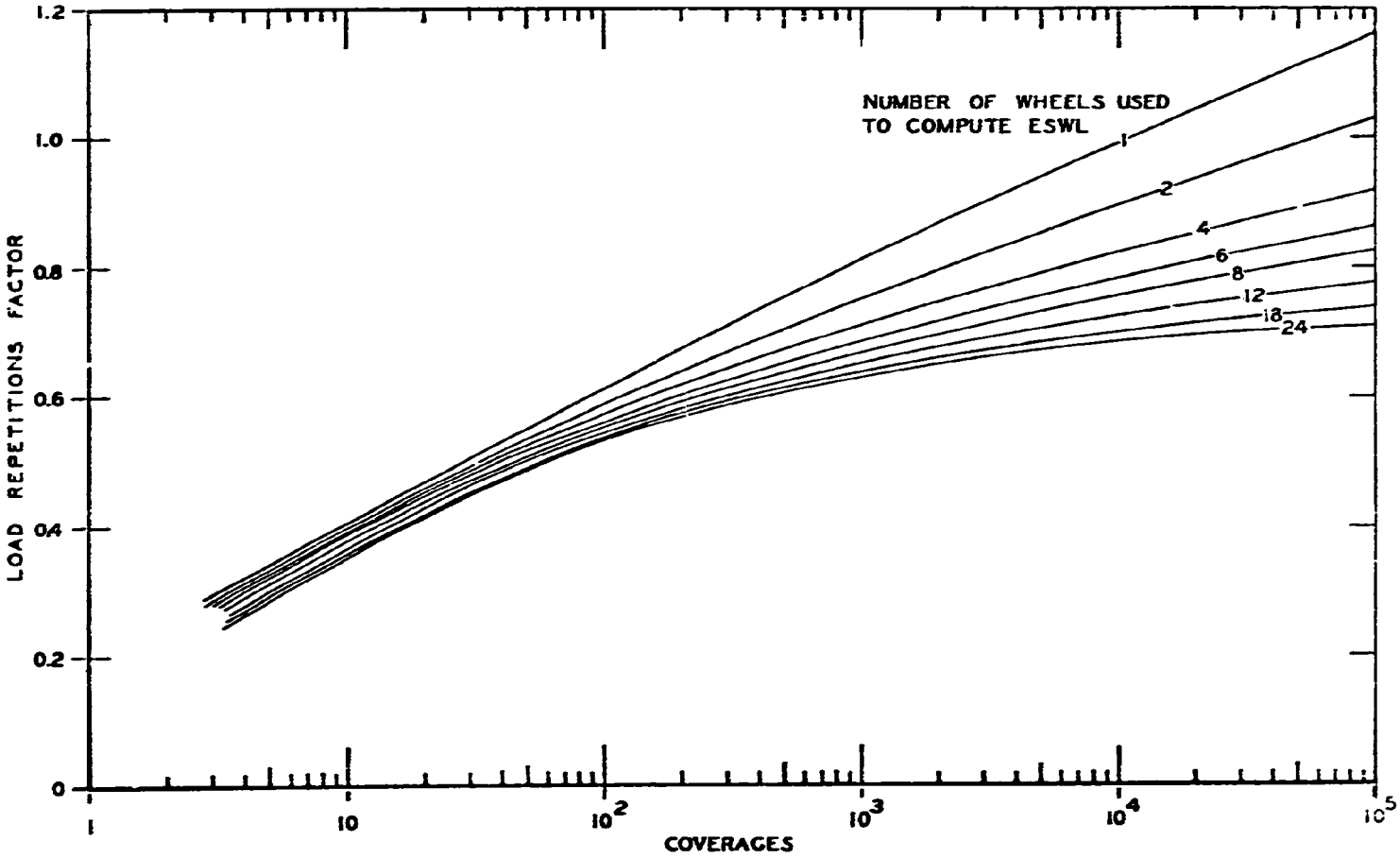

Figure 14. Load repetitions factor versus coverages for various landing gear types

test sections, show no great differences among the α values at low coverage levels. But, for large coverage levels, the difference cannot be neglected. Therefore, to use Equation 24, the α value must be taken from Figure 14 based on the anticipated number of coverages and the number of tires used to compute the ESWL. The number of tires used to compute the ESWL is that combination of tires which gives the greatest ESWL (ESWL will be discussed in Part III).

PART III: EFFECT OF WHEEL LOADS ON PAVEMENTS

Deflections in Pavements for ESWL Determinations

37. In computing elastic deflections in pavements, the CE uses mathematical expressions based on Boussinesq's one-layer theory. The pavement and the subgrade together are considered as a semi-infinite, homogeneous, isotropic, and elastic medium.

38. The deflections in the subgrade soil have been computed through the equation[11]

$$\Delta_z = \frac{pr}{E} F \tag{26}$$

where

Δ_z = the vertical deflection at a depth z, in.
p = the tire contact pressure, psi
r = the radius of the tire contact area, in.
E = the modulus of elasticity of the subgrade material, psi
F = the deflection factor (a function of the depth and the radial distance to the load center line)

39. The contact pressure is assumed to be equal to the tire inflation pressure and independent of the effect of the tire contact on the pavement surface. The tire contact area is considered to be circular, so the radius of the contact area is given by the expression

$$r = \sqrt{\frac{A_c}{\pi}} \tag{27}$$

40. Two coefficients are of particular importance in the study of deflections in earth masses: the modulus of elasticity E and Poisson's ratio ν.

41. In Equation 26, the modulus of elasticity E is considered to be constant and equal to the ratio between stress and strain, according to Hooke's law, although modern theories state that the stress-strain

relationship is nonlinear and dependent on the pressure applied to the earth mass.[12] According to the definition, the greater the modulus of elasticity, the greater the resistance of the material to elastic deformation. The modulus of elasticity of a semi-infinite half space in the one-layer theory is considered to be constant and equal to the modulus of the subgrade material.

42. Poisson's ratio is mathematically defined by the equation

$$\nu = -\frac{\varepsilon_t}{\varepsilon_1} \tag{28}$$

where ε_t is the transversal strain and ε_1 is the longitudinal strain. This coefficient expresses the ability of a material to increase its transverse dimensions when the longitudinal dimensions decrease under the effect of a compressive force, or decrease its transverse dimensions when the material is under the effect of longitudinal tensile force. It varies between 0.0 (for compressible materials) and 0.5 (for noncompressible materials). Unbound granular materials may be considered to have a variation in Poisson's ratio[13] of 0.2 to 0.5. The CE uses 0.5 as Poisson's ratio of earth materials, and this value is incorporated in the deflection factor F in Equation 26.

43. In Equation 26, the deflection factor F may be taken directly from Figure 15, prepared with Poisson's ratio equal to 0.5.

44. As part of an investigation of pressures and deflections in homogeneous soil masses at WES, Ahlvin and Ulery presented mathematical expressions from the theory of elasticity and prepared tables that permit the computation of theoretical stresses, strains, and deflections under a circular load at any place in the earth's mass, and for any value of Poisson's ratio.[14] According to Ahlvin and Ulery, the vertical deflection at a depth z is given by the expression

$$\Delta_z = p \frac{1 + \nu}{E} r \left[zA + (1 - \nu)H\right] \tag{29}$$

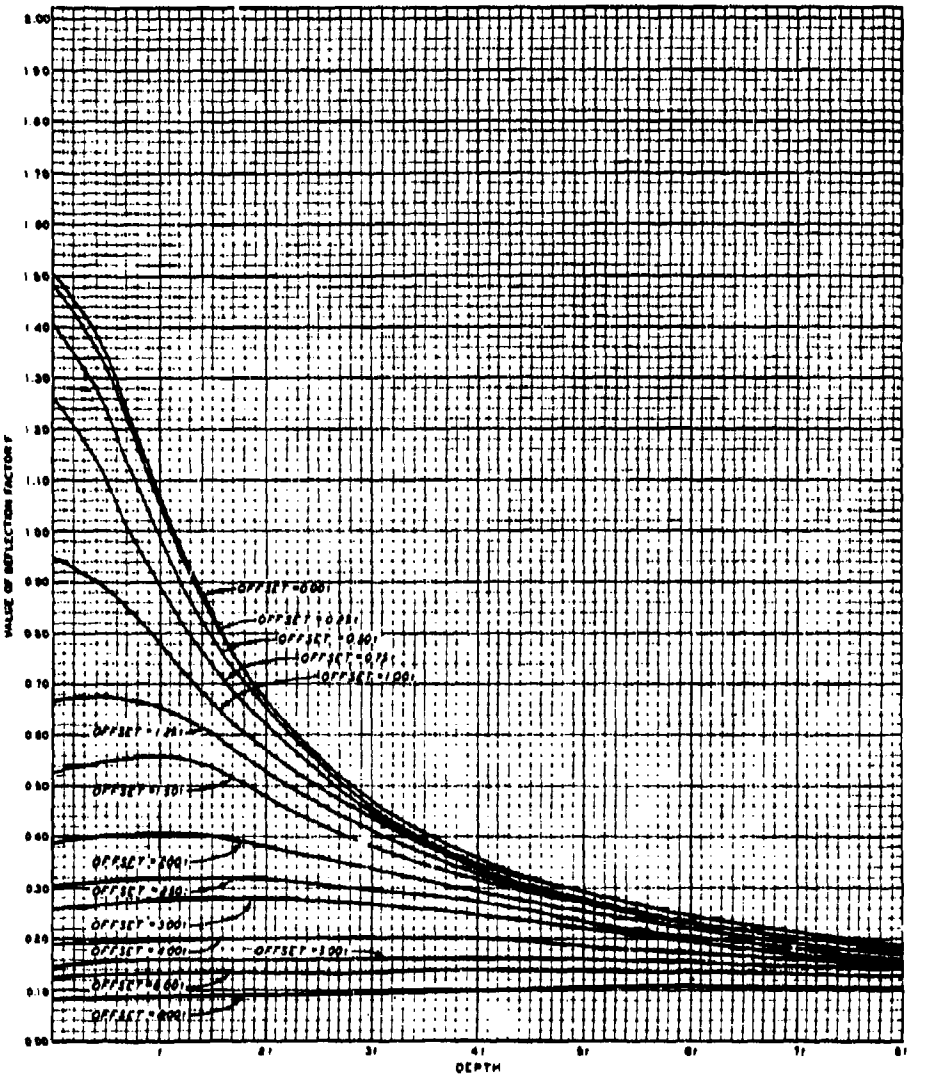

Figure 15. Deflection factor for uniform circular load and Poisson's ratio equal to 0.5

where

p, r, and E have the same meaning as in Equation 26

z = depth, in radii of the loaded area

ν = Poisson's ratio

A and H = tabulated functions shown in Tables 2 and 3

45. The above equation may be rearranged as shown below:

$$\Delta_z = \frac{pr}{E}(1 + \nu)\,[zA + (1 - \nu)H] \tag{30}$$

And, finally, the equation becomes

$$\Delta_z = \frac{pr}{E}F \tag{31}$$

where

$$F = (1 + \nu)\,[zA + (1 - \nu)H] \tag{32}$$

and represents a deflection factor that is a function of Poisson's ratio of the earth mass. Equation 32 may be written for other values of Poisson's ratio as follows:

For $\nu = 0.5$, $F = 1.5\,(zA + 0.5H)$

0.4, $F = 1.4\,(zA + 0.6H)$

0.3, $F = 1.3\,(zA + 0.7H)$

0.2, $F = 1.2\,(zA + 0.8H)$

46. Tables 4, 5, 6, and 7 show the values for Poisson's ratios of 0.5, 0.4, 0.3, and 0.2, respectively.

Single-Wheel Load

47. Deflections of earth masses under single-wheel loads may be easily computed by use of either Equation 26 with Figure 15 for Poisson's ratio equal to 0.5, or Equations 31 and 32 for any value of Poisson's ratio.

48. As expected, the deflection factors shown in Figure 15 have their maximum values at zero offset. The same may be observed in Tables 2 and 3 for values of A and H. Consequently, the maximum vertical deflection for a single-wheel load is at the center of the loaded area and this deflection diminishes with depth. Table 8 contains the maximum deflection factors for a single-wheel load, for $\nu = 0.5$, 0.4, 0.3, and 0.2. These values have been computed by use of Equation 32 and Tables 2 and 3 at zero offset. The maximum deflection factors for single-wheel loads and for $\nu = 0.5$, as used by the CE, could also be obtained from Figure 15 at zero offset or computed through the expression

$$F = \frac{3r}{3\sqrt{z^2 + r^2}} \tag{33}$$

Multiple-Wheel Load

49. Heavy loads, such as the loads transported by large aircraft, cannot be delivered to the pavement through a single wheel. Therefore, multiple-wheel assemblies are used to better distribute the loads on the pavement surface. In order to design for multiple-wheel gear loads, the concept of an "equivalent single-wheel load" was developed.[1] This concept replaces in the computations the effect of multiple wheels on the elastic medium by the effect of a single wheel. The ESWL is therefore a fictitious load acting on a single wheel that has the same contact area as one wheel of the assembly, and that produces the same deflection as the whole assembly at a given depth in the earth mass. In other words, the ESWL, acting on the pavement surface, produces at a given depth the same deflection as the multiple-wheel assembly also acting on the pavement surface.

50. In computing the ESWL, use is made of the principle of superposition,[1] which says that the effect of the whole assembly at a particular point in the earth mass is equal to the summation of the

effects of the individual tires at that point. So, for an n-wheel assembly, the following equation may be written:

$$\Delta_m = \Delta_1 + \Delta_2 + \ldots + \Delta_n \tag{34}$$

where Δ_m is the deflection due to the multiple-wheel assembly at a particular point, and Δ_1, Δ_2, ... Δ_n are the effects of the several tires of the assembly on the deflection at that point.

51. By combining Equations 32 and 34, the following equation can be written:

$$\Delta_m = \frac{pr}{E} (F_1 + F_2 \ldots + F_n) \tag{35}$$

where F_1, F_2, ... F_n are the deflection factors due to the several tires of the assembly at the point considered. Therefore,

$$\Delta_m = \frac{pr}{E} \sum_{1}^{n} F \tag{36}$$

52. Equation 36 shows the value of the deflection due to the multiple-wheel gear load at a particular point beneath the assembly. But, in the computation of the ESWL for pavement design, the maximum deflection beneath the assembly, at any depth, is needed. A family of points that represent the maximum deflection factors for the multiple-wheel load must therefore be found. If F_M represents the maximum value of $\sum_{1}^{n} F$ at any depth, Equation 36 yields:

$$\Delta_M = \frac{pr}{E} F_M \tag{37}$$

where Δ_M is the maximum deflection due to the multiple-wheel assembly at any depth under the load.

53. According to the definition of ESWL, the following equations may be written:

$$\Delta_e = \frac{p_e r}{E} F_e \tag{38}$$

and

$$\Delta_e = \Delta_M \tag{39}$$

where Δ_e is the maximum deflection due to the ESWL, p_e is the ESWL contact pressure, and F_e is the maximum deflection factor due to the ESWL. By definition, the ESWL is a single-wheel load, so its maximum deflection factor is the same as for a single wheel. Values of F_e may be taken from Tables 4, 5, 6, and 7 for $\nu = 0.5$, 0.4, 0.3, and 0.2, respectively.

54. Equations 37, 38, and 39 combined yield

$$\frac{pr}{E} F_M = \frac{p_e r}{E} F_e \tag{40}$$

or

$$F_e = p \frac{F_M}{F_e} \tag{41}$$

Since the contact area of the ESWL is equal to the contact area of one wheel of the assembly, the following equations may be written:

$$p_e A_c = p A_c \frac{F_M}{F_e} \tag{42}$$

and

$$P_e = P \frac{F_M}{F_e} \tag{43}$$

55. Equation 43 shows the relationship between the ESWL (P_e) and the load on one tire of the multiple-wheel assembly (P). The ESWL is

not a constant, but varies with the deflection factor ratio $\frac{F_M}{F_e}$. As considered by the CE for pavement purposes, the deflection factor ratio and consequently the ESWL vary with depth only.

Computation of ESWL

56. To compute the ESWL for a particular multiple-wheel assembly, the following data must be known: type of assembly, wheel spacing, assembly load, tire contact area or tire pressure, and Poisson's ratio of the subgrade material. As mentioned earlier, the CE uses a Poisson's ratio of 0.5 for materials used in conventional flexible pavements.

57. Equation 43 shows the ESWL to be a function of the load on one wheel of the assembly and the ratio of the maximum deflection factor for the multiple wheels and the maximum deflection factor for the single wheel. The F_e value is easily obtained, as discussed in previous paragraphs. To compute F_M, the following steps are taken:

a. Compute the maximum deflection factors beneath one wheel of the assembly, as follows: (1) select a wheel and list its maximum deflection factors (from Table 8) for several depths, and (2) determine the deflection factors for the other wheels of the assembly at their offset distances (Tables 4, 5, 6, or 7). The summation of the deflection factors thus obtained, at each depth considered, represents the maximum deflection factors beneath one wheel at several depths and yields the maximum deflection factors curve for one wheel of the assembly.

b. Compute the maximum deflection factors beneath the critical points. Each configuration must be analyzed on a case-by-case basis. For example, for a dual-wheel assembly, the critical point is midway between the two wheels. Beneath a twin-tandem, the maximum deflection migrates with depth, from a point beneath the center of one tire contact area at the pavement surface to the centroid of the assembly at deep depths. This migration follows a curved path whose shape depends on the gear geometry. Therefore, the centroid of the assembly and a point where, according to good judgment, the flow path is considered to be must be chosen as critical points.

c. The maximum deflection factors beneath one wheel and beneath the critical points are plotted and the respective

curves must be drawn. The maximum deflection factor beneath one wheel is the maximum at shallow depths. At deep depths, the F_M value lies beneath the centroid of the gear. Thus, the curves will intersect at some depth. That portion of each curve in the vicinity of this intersection must be interconnected by a smooth curve[1] to represent the maximum F_M values at all depths (Figure 16).

58. In a previous paragraph, it was stated that the ESWL varies with depth. Therefore, the usual procedure is to compute the ESWL as a percent of the assembly load and then plot this percent versus depth (Figure 17).

Example of ESWL Computation

59. Compute the ESWL for a C-131E aircraft which has the following characteristics:[15]

Type of assembly: Twin

Wheel spacing: 26 in.

Assembly load: 27,000 lb (45 percent of the maximum gross weight)

Tire pressure: 90 psi

Poisson's ratio of the subgrade material: 0.4

60. The following steps should be followed in computing the ESWL:

a. Compute the load on one tire, P . Since the assembly has twin wheels,

$$P = \frac{\text{Assembly load}}{2} = \frac{27,000 \text{ lb}}{2} = 13,500 \text{ lb}$$

b. Determine the maximum deflection factors for a single wheel.

61. The maximum deflection factors F_e for a single wheel may be taken directly from Table 8 for the value of $\nu = 0.4$. The depth in radii is converted to inches as follows:

a. Calculate the tire contact area A_c :

$$A_c = \frac{P}{p} = \frac{13,500}{90} = 150 \text{ sq in.}$$

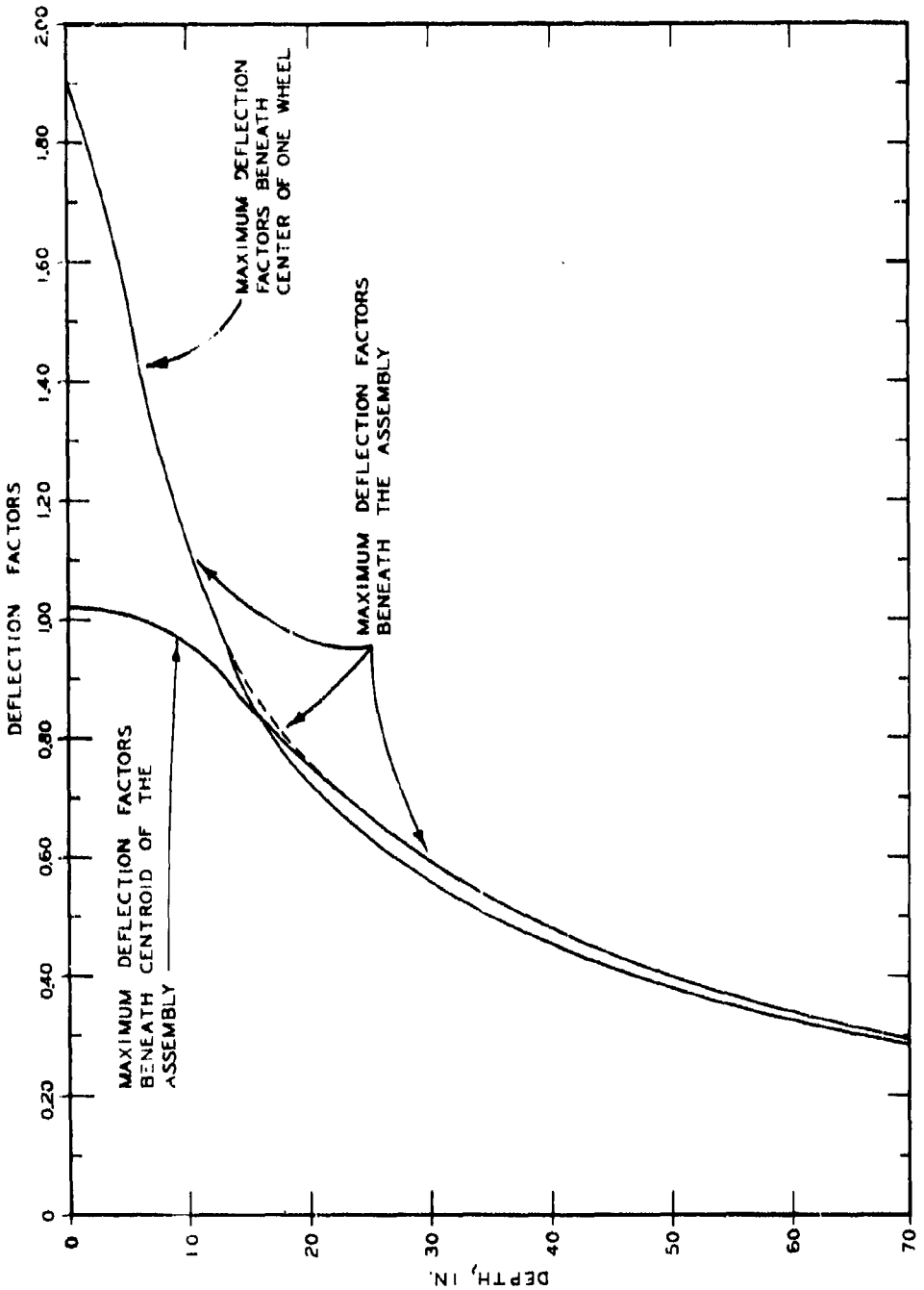

Figure 16. Maximum deflection factors for the C-131E aircraft

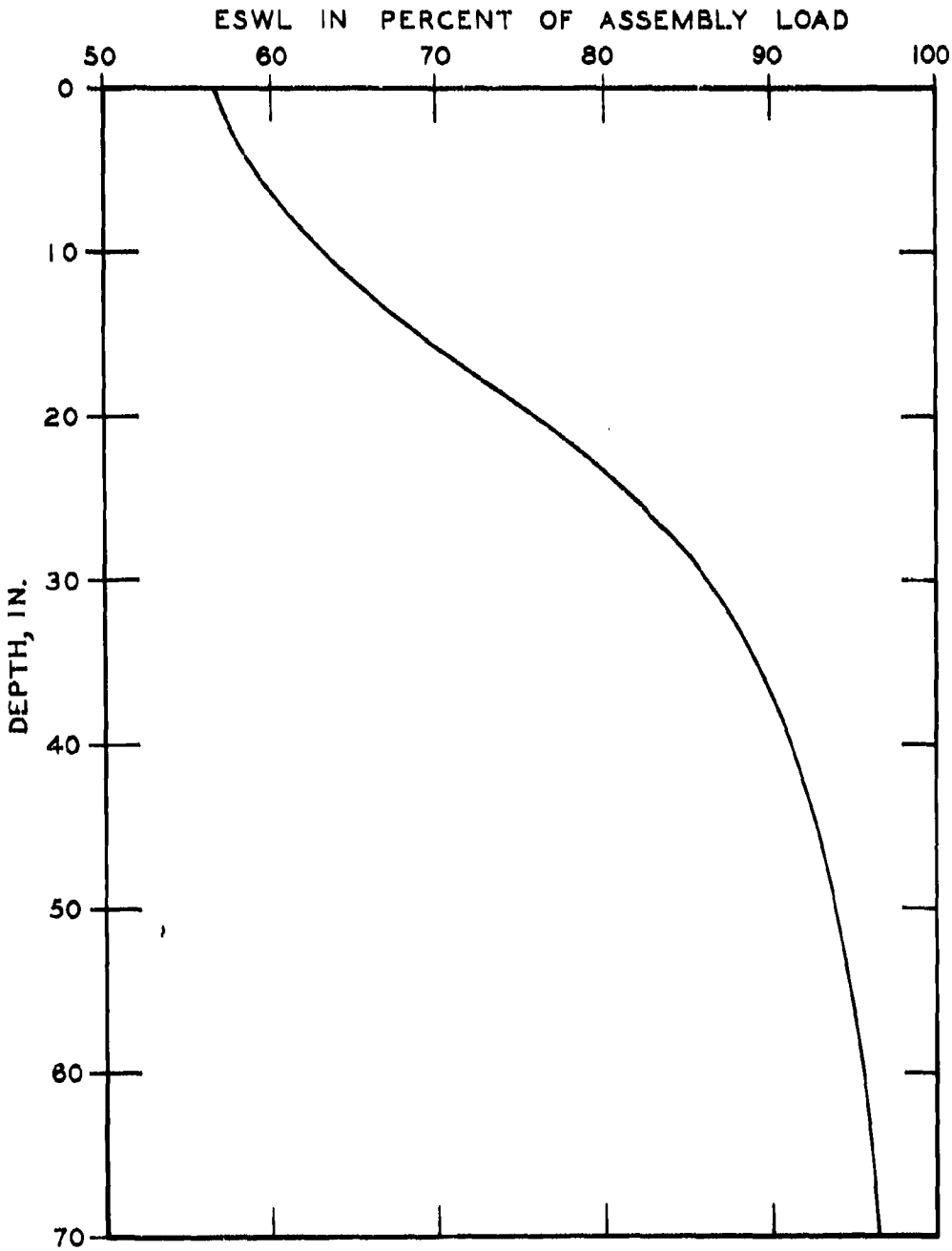

Figure 17. ESWL curve for the C-131E aircraft

where

P = load on one tire, lb

p = tire pressure, psi

b. The contact area is considered to be circular and the radius of the area is determined:

$$r = \sqrt{\frac{A_c}{\pi}} = 6.91 \text{ in.}$$

62. The values of the maximum deflection factors for a single wheel and for a Poisson's ratio of 0.4 are listed again in Table 9.

63. Determine the maximum deflection factors for the multiple-wheel gear as follows:

a. The maximum deflection factors beneath one wheel of the assembly must be determined. For the twin assembly, the maximum deflection factor directly under one wheel is the summation of the effects of both wheels at the center line of one of them. In other words, the maximum deflection beneath one wheel is equal to the maximum deflection under a single wheel, plus the deflection produced under that wheel by the other wheel. The maximum deflection factors beneath a single wheel may be taken directly from Table 8. The distance between the two wheels is 26 in., or 3.76 radii. Therefore, the deflection factors at the offset distance of the other wheel may be taken from Table 5, through a linear interpolation, for an offset distance equal to 3.76 radii. These values are shown in Table 10.

b. The maximum deflection factors midway between the two wheels of the twin assembly must now be found. This point corresponds to an offset distance of 1.88 radii from each wheel. These factors are shown in Table 11.

c. Curves can be drawn (Figure 16) using the values of F_M computed beneath one wheel and beneath the centroid of the assembly. These two curves are then connected by drawing a smooth curve at the point of intersection of the two curves. This combined curve represents the maximum deflection factors under the C-131E aircraft.

64. The ESWL can now be computed using the deflection factors taken from the maximum deflection factor curve (see Table 12). A curve of the ESWL in percent of assembly load can now be constructed, as presented in Figure 17.

PART IV: CONSTRUCTION OF CBR DESIGN CURVES

CBR Equation

65. The purpose of a pavement is to protect the subgrade from shear failure due to the loads applied at the pavement surface. These loads are applied through tires to the pavement, which spreads the stresses to the point where they do not exceed the strengths of the various pavement layers or the subgrade. Therefore, data such as magnitude of load, tire arrangement, the number of repetitions, and the soil strength are of primary importance for pavement design.

66. The CE uses CBR as a measure of soil strength. It is obtained by use of a standardized test method that gives an indication of the resistance of a soil to the penetration of a piston having an end area of 3 sq in. The CBR is a percentage of a standard resistance[4,16] but is presented as a dimensionless index number.

67. In Part II of this report it was shown that the design thickness of a pavement was equal to a standard thickness, T, corrected by a load repetitions factor, α. In recent years, this standard thickness has been computed using the following CBR equation, which was adequate for low strengths but which had to be modified in the high strength range for pavement stability and longevity.

$$T = \sqrt{\frac{P}{8.1\ CBR} - \frac{A_c}{\pi}} \tag{44}$$

In this equation, T is the thickness in inches; P is measured in pounds and represents the tire load for a single-wheel gear, or the ESWL for multiple-wheel loads; and A_c is the tire contact area in square inches, usually considered equal to the quotient of the tire load and the tire pressure.

68. This equation was developed primarily from performance data but makes some use of theoretical concepts. It was developed from actual data taken from test sections and airfields in use, with some consideration of the pattern of stresses under a uniform circular load in a

homogeneous, isotropic, and elastic half space. The mathematical developments leading to the CBR equation may be found in Reference 2.

69. Equation 44 can also be written as follows:

$$T = \sqrt{P\left(\frac{1}{8.1\ CBR} - \frac{1}{p\pi}\right)} \tag{45}$$

where p is the average tire contact pressure in psi. And, finally, Equation 45 may be expressed in terms of two parameters, $\frac{T}{\sqrt{A_c}}$ and $\frac{CBR}{p}$, as follows:

$$\frac{T}{\sqrt{A_c}} = \sqrt{\frac{1}{8.1\ \frac{CBR}{p}} - \frac{1}{\pi}} \tag{46}$$

The above parameters can be plotted as a combined CBR curve as shown in Figure 18.

70. An analysis of Equation 46 shows the parameter $\frac{T}{\sqrt{A_c}}$ to have real values in the interval

$$0 < \frac{CBR}{p} \leq 0.39$$

71. For the upper values of $\frac{CBR}{p}$, the value of $\frac{T}{\sqrt{A_c}}$ approaches zero, which indicates that the underlying layer is sufficiently strong and does not need a pavement layer to protect it.[2] However, in practice, a minimum thickness of pavement is required to provide a wearing surface and durability. The CBR curve can be adjusted to incorporate these minimum thickness requirements.[1]

72. Recently, a new $\frac{CBR}{p}$ versus $\frac{T}{\sqrt{A_c}}$ relation was developed using data from extensive tests conducted at WES with multiple-wheel heavy gear loads,[9,10] as well as data from earlier test sections.[3] The new curve (Figure 19) coincides with the curve shown in Figure 18 for the lower values of $\frac{CBR}{p}$. The statistical equation of the best-fit curve, in terms of the same parameters $\frac{CBR}{p}$ and $\frac{T}{\sqrt{A_c}}$, is:

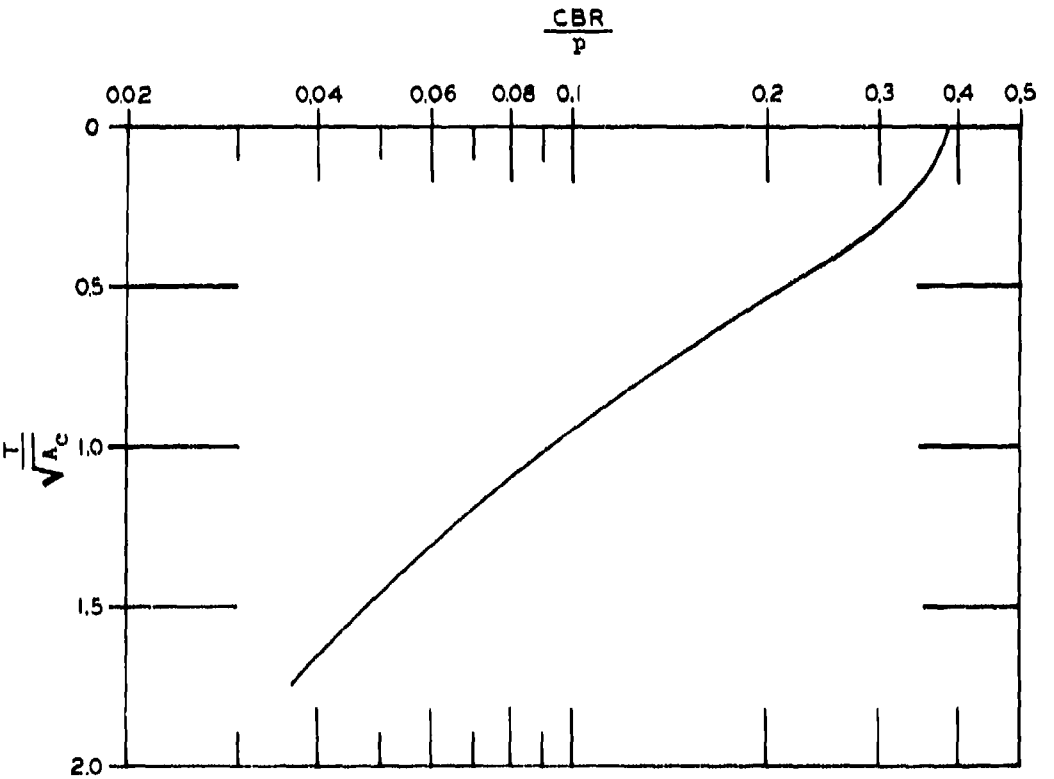

Figure 18. Curve from CBR equation

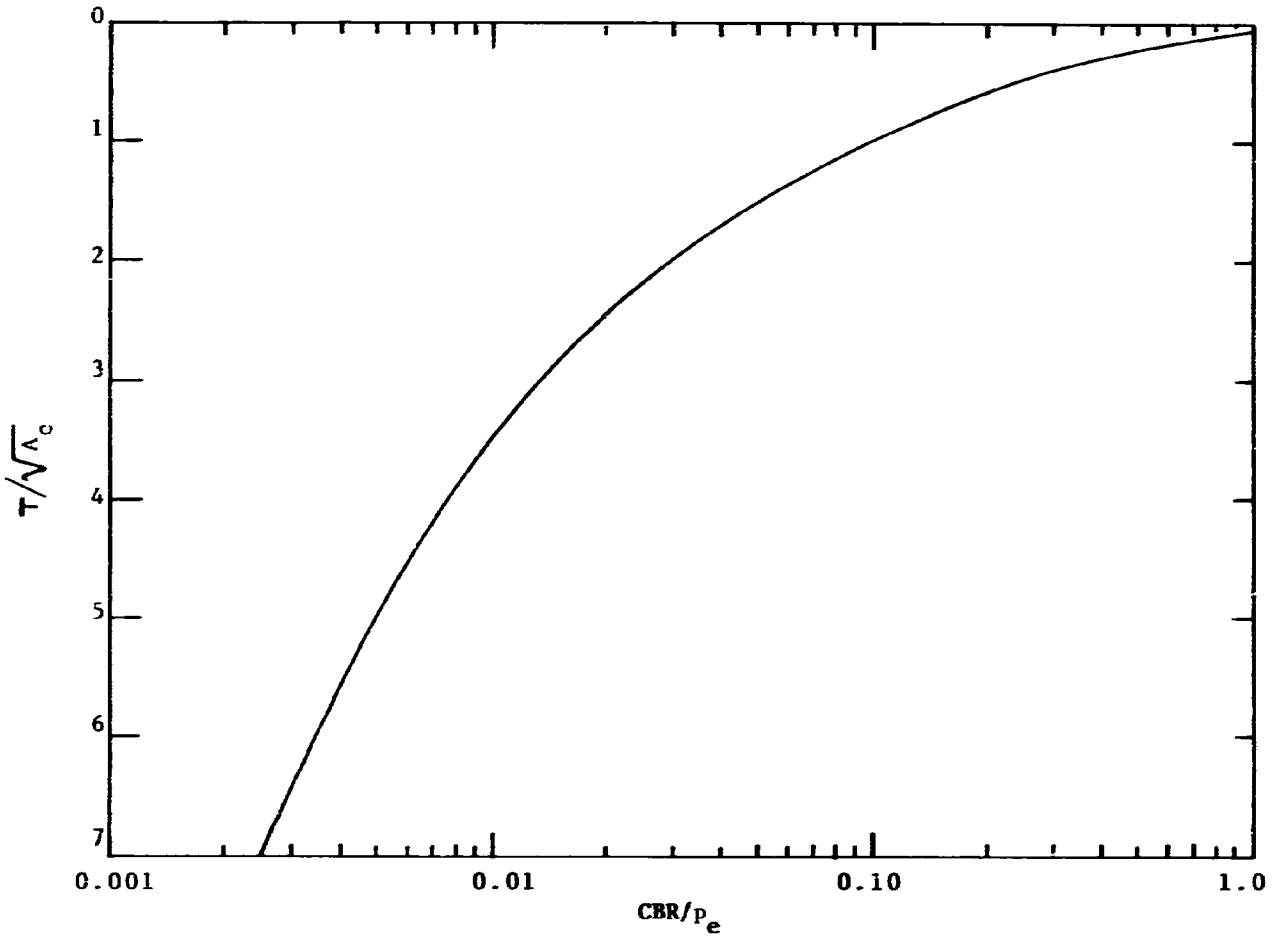

Figure 19. $\frac{T}{\sqrt{A_c}}$ versus $\frac{CBR}{p_e}$

$$\frac{T}{\sqrt{A_c}} = \left[- 0.0481 - 1.562 \left(\log \frac{CBR}{p}\right) - 0.6414 \left(\log \frac{CBR}{p}\right)^2 - 0.4730 \left(\log \frac{CBR}{p}\right)^3 \right] \quad (47)$$

Both Equation 47 and the curve in Figure 19 can be used to compute the pavement thickness for any value of CBR. No adjustment of this curve is required for the higher values of $\frac{CBR}{p}$.

73. Equations 44 and 45, as well as the curve in Figure 18, may still be used in computing pavement thickness on subgrades with CBR values up to about 12-15.

74. The computation of pavement thickness for single-wheel loads may be done by direct use of the above methodology. The computation of pavement thickness for multiple-wheel loads may be accomplished in a manner similar to that for single-wheel loads, but since the ESWL does not have a fixed value and instead varies with depth, the value to be used in the CBR equation must be determined for the pavement thickness. Two situations are normally considered in determining the CBR/thickness relationship as follows:

a. When the CBR of the underlying layer is known, the thickness of pavement is computed. For single wheels, this can be accomplished directly through use of the equations. However, for multiple-wheel loads an iterative procedure is required. In this procedure, a thickness is assumed and the corresponding ESWL and tire pressure are computed. Then, by use of Figure 19, a value of thickness can be computed. This result is then compared with the assumed value. If they are not sufficiently close, a new thickness is assumed, close to the computed thickness, and the calculations repeated. When the assumed and computed values are sufficiently close, the CBR equation or its curve and ESWL have been properly used.

b. When the thickness is fixed and the CBR is desired, the ESWL at the fixed depth can be computed and no trial-and-error procedure is involved in the use of the CBR equation or its curve.

CBR Design Curves for Aircraft

75. A set of design curves may be constructed based upon the procedures presented above, by repeating the calculations for various loads, traffic levels, or thicknesses. The calculations may be made simpler when numerous values are needed by assuming the pavement thicknesses and calculating the CBR required. This eliminates the trial-and-error procedures. Part V of this report has been prepared in order to illustrate the development of a set of design curves through application of the entire procedure presented herein.

PART V: COMPLETE EXAMPLE OF THE CONSTRUCTION OF CBR DESIGN CURVES FOR AIRFIELDS

Introduction

76. This part was prepared in order to show a complete example of the development of CBR design curves for flexible pavements. This example will be for the C-141A aircraft, which is currently used by the Air Force for the design of medium-load airfields.

Example Problem

77. Assume a set of design curves for taxiways is desired for 10,000, 50,000, and 100,000 passes of the C-141A aircraft having the following characteristics:

Gear configuration: Twin-tandem tricycle (Figure 20)
Wheel spacing: 32.5 by 48.0 in.
Tread (T_w): 210 in.
Tire width (W_t): 12.6 in.
Tire contact area (A_c): 208 sq in.
Maximum takeoff weight: 320.0 kips

Poisson's ratio is assumed to be 0.5.

78. The solution of this problem may be divided into three parts: (a) computation of the pass-per-coverage ratio, (b) computation of the ESWL, and (c) computation of thickness requirements.

Computation of pass-per-coverage ratio

79. Since the main gear is a twin-tandem arrangement, the pass-per-coverage ratio is given by Equation 23:

$$\frac{P}{C} = \frac{1}{f(x_{oc})\ W_t}$$

where $f(x_{oc})$ is the maximum ordinate of the cumulative distribution curve and W_t is the tire width.

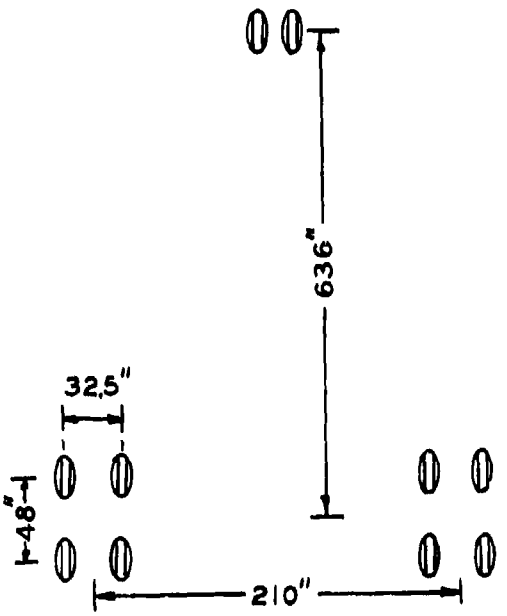

Figure 20. C-141A landing gear configuration

80. A twin-tandem assembly is composed of two twin wheels in tandem, having the same wheel path and producing identical cumulative distribution curves. Therefore, the ordinates of a twin-tandem cumulative distribution curve equal two times the corresponding ordinates of the cumulative curve of one of the twins. The cumulative curve of a twin is obtained by graphical addition of the overlapping ordinates of two adjacent GND curves for one wheel, separated by a distance equal to the wheel spacing.

81. The ordinates of a GND curve of one wheel are given by Equation 4.

$$f(x) = \frac{1}{\sigma_x} f(z)$$

According to Equation 16, for a wander width equal to 70 in., used currently for taxiways, σ_x equals 30.43 in. The values of z and

$f(z)$ may be taken from Table 1. Table 13 may then be prepared for the construction of the GND curve for one wheel.

82. Using the values in Table 13, two equal curves can be drawn (Figure 21) 32.5 in. apart to represent the effect of the front or rear twin wheels. Each solid line represents one wheel. The dashed line represents the cumulative curve for the two wheels. The cumulative value of the ordinates for the twin-tandem is double the value of the dashed line. So,

$$f(x_{oc}) = 2 \times 0.0231 = 0.0462$$

83. Since the wander is 70 in. and the spacing between the center lines of inside wheels $(T_W - S_t)$ is greater than 100 in., the cumulative curves of one twin-tandem gear will have no influence on the other. Therefore, the maximum ordinate for the C-141A aircraft is $f(x_{oc}) = 0.0462$.

84. The maximum ordinate could also be found in a simple manner by use of the chart in Figure 10, without need of constructing the GND curves.

85. With the known values of $f(x_{oc})$ and W_t , the pass-per-coverage ratio can be computed, as follows:

$$\frac{P}{C} = \frac{1}{0.0462 \times 12.6} = 1.72$$

Computation of ESWL

86. The ESWL is computed through Equation 43:

$$P_e = P \frac{F_M}{F_e}$$

where P is the load on one wheel of the assembly, F_M is the maximum deflection factor for the multiple-wheel assembly, and F_e is the single-wheel maximum deflection factor. This example will be for one main landing gear consisting of four tires.

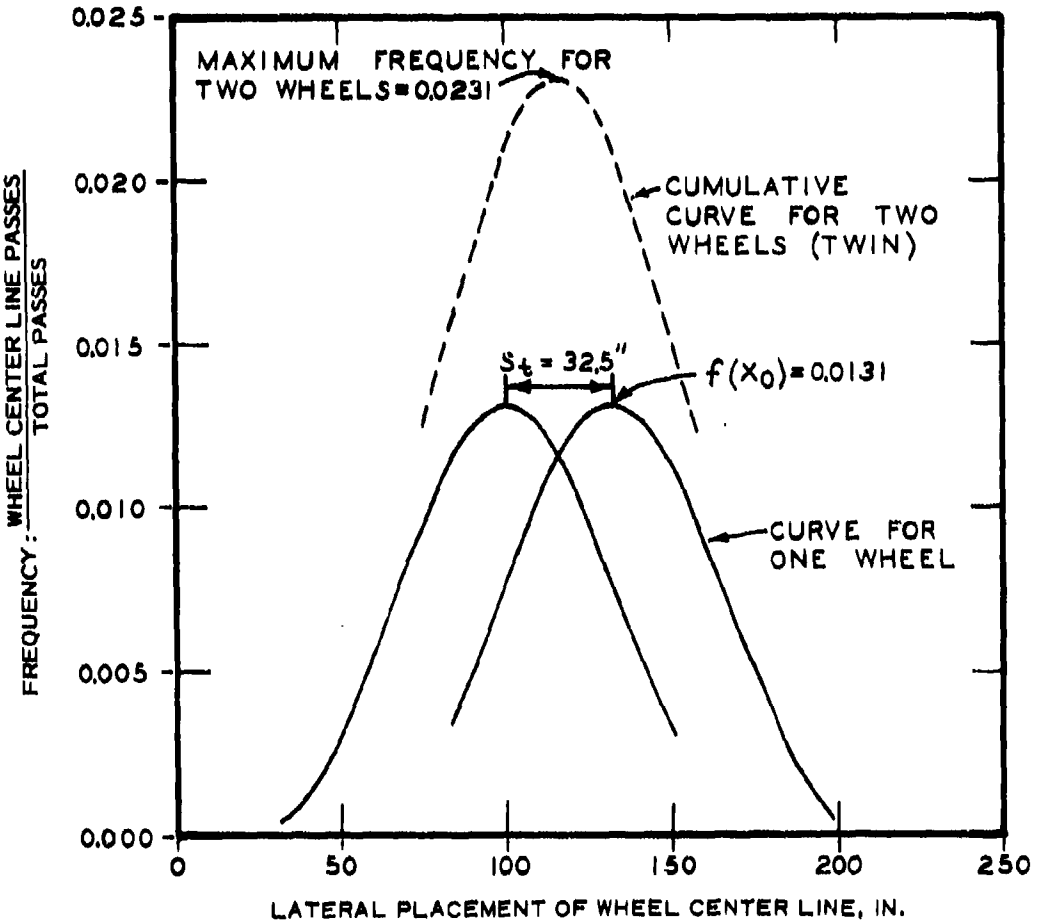

Figure 21. GND curve, front or rear twin of the C-141A main gear

a. Determine the load on one wheel (P). The load on one main gear of the C-141A is considered equal to 45 percent of the aircraft gross weight. Since the assembly has four tires, P may be computed as shown below:

$$P = \frac{1}{4} \times 0.45 \times 320{,}000 = 36{,}000 \text{ lb}$$

b. Determine single-wheel deflection factors. The ESWL is, by definition, a single-wheel load; therefore, the maximum deflection factors for a single wheel (F_e) may be taken from Table 8 for $\nu = 0.5$. Since the tire contact area is considered circular, the radius is:

$$r = \sqrt{\frac{A_c}{\pi}} = \sqrt{\frac{208}{\pi}} = 8.14 \text{ in.}$$

The F_e values for various depths taken from Table 8 relate to depth as shown in Table 14.

c. Determine maximum multiple-wheel deflection factors.

(1) The first step in determining the maximum deflection factors for a multiple-wheel assembly is to compute the deflection factors beneath one wheel of the assembly (point 1, Figure 22). For a twin-tandem gear, the maximum deflection factors beneath one wheel are the summation of the maximum deflection factors produced by one wheel (zero offset) plus the deflection factors produced by the other wheels at their offset distances.

(2) The maximum deflection factors beneath one wheel at zero offset may be taken from Table 8. The maximum deflection factors at the offset distances of the other wheels may be taken from Table 4, by linear interpolation. For the offset distances of 32.5 in. or 3.99 radii, 48.0 in. or 5.90 radii, and 47.96 in. or 7.12 radii, the deflection factors will be as shown in Table 15.

(3) The second step is to compute the deflection factors at the centroid of the assembly (point 2 in Figure 22), or at 3.56 radii from all wheels. The deflection factors at this point due to the whole assembly equal four times the factor for one wheel. Table 16 shows the maximum deflection factors at the centroid of the assembly obtained from Table 4.

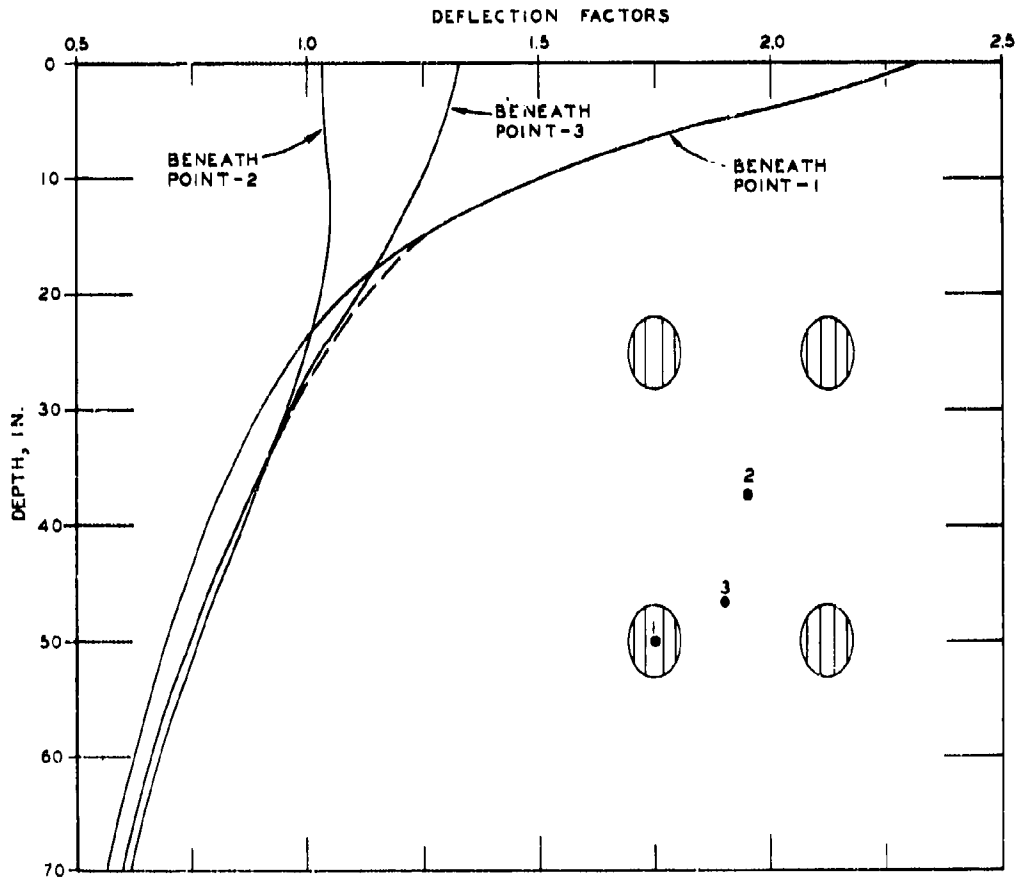

Figure 22. Maximum deflection factor curves

(4) The two points considered above are the easiest to identify as critical points under any kind of gear. It is known that, under a twin-tandem assembly, the maximum deflection factors migrate with depth, through a curve starting just beneath the center of one wheel and ending beneath the centroid of the assembly. This path varies according to the gear geometry, and there is no practical way to identify it. Therefore, a third point is selected arbitrarily, where the migration path is more likely to be. This third point helps to construct the final maximum deflection curves, given basically by the first two curves. It may be necessary at times to select more than three points to fully define the maximum deflection curve.

(5) Select an intermediate point (point 3 in Figure 22) whose offset distances to the four wheels are 14 in. or 1.72 radii, 21 in. or 2.58 radii, 43 in. or 5.28 radii, and 46 in. or 5.61 radii. Table 17 shows the deflection factors for this point.

(6) The next step is to draw the deflection factor curves corresponding to the critical points studied (Figure 22). As can be seen, at shallow depths the deflection factors are maximum at point 1. At deep depths, the maximum deflection factors occur at point 2. At intermediate depths, the maximum deflection factors occur at point 3, which assists in construction of a dashed curve that provides a transition between the other curves. The combined curve represents the maximum deflection factors beneath the assembly. With values taken from this curve, the ESWL corresponding to various depths can be computed.

(7) The ESWL is usually computed in percent of the assembly load. Table 18 can help in the computations. Using these values, a curve of the ESWL in percent of the assembly load versus depth can be constructed, as shown in Figure 23.

(8) This procedure may be followed for other groupings of tires to insure that the maximum ESWL has been obtained.

Determination of CBR/thickness requirements

87. The CBR versus thickness curves may be developed for any loading condition. This example is for the C-141A and the calculations herein are for a 320,000-lb gross weight. The calculation of the CBR-thickness relationships may be accomplished by hand calculations or by computer. Both methods will be presented in this report. Appendix A

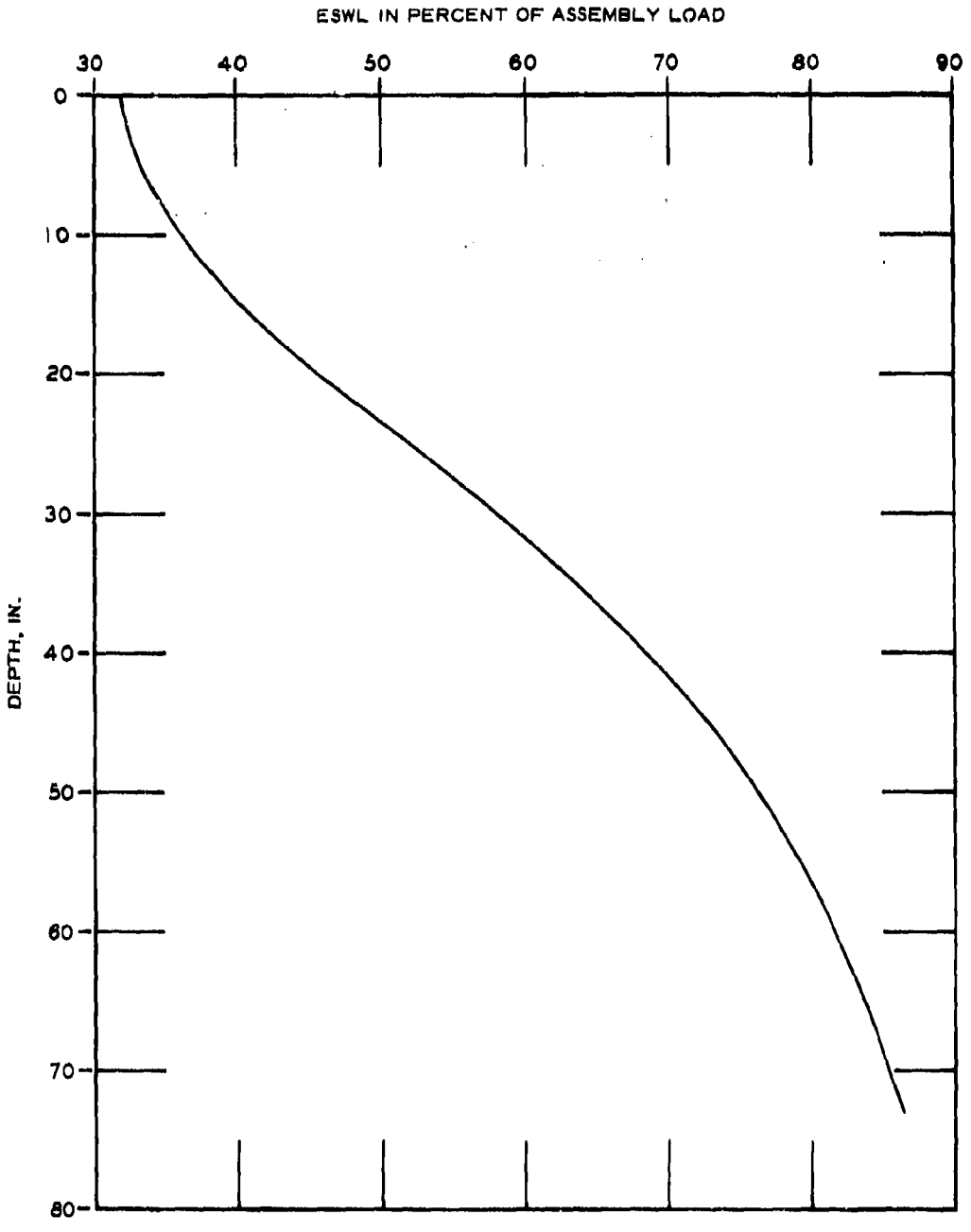

Figure 23. ESWL curve for the C-141A

contains the procedures for determining thickness requirements using the computer program. This portion of the report will present the hand method of calculation, which follows several distinct steps. These steps are illustrated in Tables 19, 20, and 21, which present calculations for 10,000, 50,000, and 100,000 passes.

a. Step 1. The initial step in the procedure is to assume a series of thicknesses for which it is desired to calculate the corresponding CBR values.

b. Step 2. The second step is to convert the thicknesses assumed above for particular pass levels to standard thicknesses using the load repetition factors (α) from Figure 14. This figure is presented in terms of coverages; therefore, the number of passes must be converted to coverages using the pass-per-coverage ratio of 1.72 calculated previously for the C-141A. The 10,000 passes convert to 5,814 coverages and yield an α of 0.791, the 50,000 passes convert to 29,069 coverages and yield an α of 0.87, and the 100,000 passes convert to 58,140 coverages and yield an α of 0.90.

c. Step 3. The standard thicknesses are divided by the square root of the contact area. The $\frac{T}{\sqrt{A_c}}$ values are then used to enter Figure 19 and corresponding values of $\frac{CBR}{p_e}$ are determined.

d. Step 4. Determine the ESWL at the assumed depths using values of ESWL as a percent of the assembly load obtained from Figure 23. Divide the ESWL by the contact area of one tire to obtain the ESWL tire pressure (p_e).

e. Step 5. The $\frac{CBR}{p_e}$ values are then multiplied by the corresponding p_e values to obtain the CBR required below the assumed thickness.

88. This procedure is repeated for each desired load or pass level. The final CBR versus thickness curves can now be plotted for each pass level as shown in Figure 24.

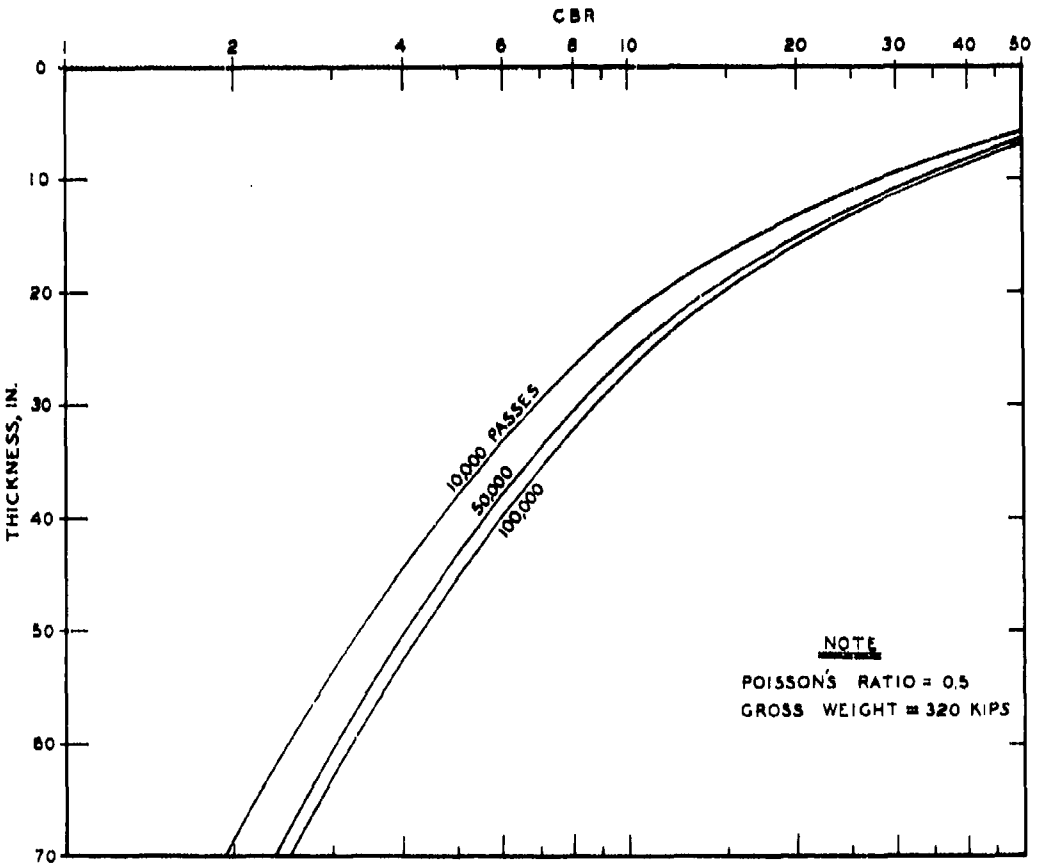

Figure 24. CBR/thickness design curves for the C-141A aircraft

REFERENCES

1. Ahlvin, R. G., "Developing a Set of CBR Design Curves," Instruction Report 4, Nov 1959, U. S. Army Engineer Waterways Experiment Station, CE, Vicksburg, Miss.

2. Turnbull, W. J., Foster, C. R., and Ahlvin, R. G., "Mathematical Expression of the CBR Relations," Technical Report No. 3-441, Nov 1956, U. S. Army Engineer Waterways Experiment Station, CE, Vicksburg, Miss.

3. Ahlvin, R. G., "Consolidated CBR Criteria," Journal, Soil Mechanics and Foundations Division, American Society of Civil Engineers, Vol 84, SM4, Oct 1958, pp 1825-1 - 1825-16.

4. "Development of CBR Flexible Pavement Design Method for Airfields (A Symposium)," Transactions, American Society of Civil Engineers, Vol 115, Paper 2406, 1950, p 453.

5. Turnbull, W. J., Foster, C. R., and Ahlvin, R. G., "Design of Flexible Airfield Pavements for Multiple-Wheel Landing Gear Assemblies; Analysis of Existing Data," Technical Memorandum No. 3-349, Report 2, Jun 1955, U. S. Army Engineer Waterways Experiment Station, CE, Vicksburg, Miss.

6. Brown, D. N. and Thompson, O. O., "Lateral Distribution of Aircraft Traffic," Miscellaneous Paper S-73-56, Jul 1973, U. S. Army Engineer Waterways Experiment Station, CE, Vicksburg, Miss.

7. Spiegel, M. R., Schaum's Outline of Theory and Problems of Statistics, Schaum Publishing, New York, 1961.

8. Arkin, H. and Colton, R. R., Statistical Methods, 5th ed., Barnes and Noble, New York, 1970.

9. Ahlvin, R. G. et al., "Multiple-Wheel Heavy Gear Load Pavement Tests; Basic Report," Technical Report S-71-17, Volume I, Nov 1971, U. S. Army Engineer Waterways Experiment Station, CE, Vicksburg, Miss.

10. Hammitt, G. M. et al., "Multiple-Wheel Heavy Gear Load Pavement Tests; Analysis of Behavior Under Traffic," Technical Report S-71-17, Volume IV, Nov 1971, U. S. Army Engineer Waterways Experiment Station, CE, Vicksburg, Miss.

11. U. S. Army Engineer Waterways Experiment Station, CE, "Investigations of Pressures and Deflections for Flexible Pavements; Homogeneous Clayey-Silt Test Section," Technical Memorandum No. 3-323, Report 1, Mar 1951, Vicksburg, Miss.

12. Sowers, G. F. and Vesic, A. B., "Vertical Stresses in Subgrades Beneath Statically Loaded Flexible Pavements," Stress Distribution in Earth Masses, Bulletin 342, pp 90-120, 1962, Highway Research Board, National Academy of Sciences - National Research Council, Washington, D. C.

13. Yoder, E. J. and Witczak, M. W., Principles of Pavement Design, 2d ed., Wiley, New York, 1975.

14. Ahlvin, R. G. and Ulery, H. H., "Tabulated Values for Determining the Complete Pattern of Stresses, Strains, and Deflections Beneath a Uniform Circular Load on a Homogeneous Half Space," Stress Distribution in Earth Masses, Bulletin 342, pp 1-13, 1962, Highway Research Board, National Academy of Sciences - National Research Council, Washington, D. C.

15. Hay, D. R., "Aircraft Characteristics for Airfield Pavement Design and Evaluation," Technical Report No. AFWL-TR-69-54, Oct 1969, Air Force Weapons Laboratory, Kirtland Air Force Base, N. Mex.

16. Department of Defense, "Test Method for Pavement Subgrade, Subbase, and Base-Course Materials," Military Standard Mil-Std-621A, Dec 1964, Washington, D. C.

Table 1

Ordinates and Area Under the SND Curve

z in standard deviations	f(z)	Area Under the Curve percent
0.00	0.3989	0.00
0.20	0.3910	7.93
0.50	0.3521	19.15
1.00	0.2420	34.13
1.15	0.2059	37.49
1.50	0.1295	43.32
2.00	0.0540	47.72
3.00	0.0044	49.87
3.99	0.0001	50.00

Table 2

Function "A"

Depth z in radii	Offset in radii 0	0.2	0.4	0.6	0.8	1	1.2	1.5	2	3	4	5	6	7	8	10	12	14
0	1.0	1.0	1.0	1.0	1.0	.5	0	0	0	0	0	0	0	0	0	0	0	0
0.1	.90050	.89748	.88679	.86126	.78797	.43015	.09645	.02787	.00856	.00211	.00084	.00042						
0.2	.80388	.79824	.77884	.73483	.63014	.38269	.15433	.05251	.01680	.00419	.00167	.00083	.00048	.00030	.00020			
0.3	.71265	.70518	.68316	.62690	.52081	.34375	.17964	.07199	.02440	.00622	.00250							
0.4	.62861	.62015	.59241	.53767	.44329	.31048	.18709	.08593	.03118									
0.5	.55279	.54403	.51622	.46448	.38390	.28156	.18556	.09499	.03701	.01013	.00407	.00209	.00118	.00071	.00053	.00025	.00014	.00009
0.6	.48550	.47691	.45078	.40427	.33676	.25588	.17952	.10010										
0.7	.42654	.41874	.39491	.35428	.29833	.23311	.17124	.10228	.04558									
0.8	.37531	.36832	.34729	.31243	.26581	.21297	.16206	.10236										
0.9	.33104	.32492	.30669	.27707	.23832	.19488	.15253	.10094										
1	.29289	.28763	.27005	.24697	.21468	.17868	.14329	.09849	.05185	.01742	.00774	.00393	.00226	.00143	.00097	.00050	.00029	.00018
1.2	.23178	.22795	.21662	.19890	.17626	.15101	.12570	.09192	.05260	.01935	.00871	.00459	.00269	.00171	.00115			
1.5	.16795	.16552	.15877	.14804	.13436	.11892	.10296	.08048	.05116	.02142	.01013	.00548	.00325	.00210	.00141	.00073	.00043	.00027
2	.10557	.10453	.10140	.09647	.09011	.08269	.07471	.06275	.04496	.02221	.01160	.00659	.00399	.00264	.00180	.00094	.00056	.00036
2.5	.07152	.07098	.06947	.06698	.06373	.05974	.05555	.04880	.03787	.02143	.01221	.00732	.00463	.00308	.00214	.00115	.00068	.00043
3	.05132	.05101	.05022	.04886	.04707	.04487	.04241	.03839	.03150	.01980	.01220	.00770	.00505	.00346	.00242	.00132	.00079	.00051
4	.02986	.02976	.02907	.02802	.02832	.02749	.02651	.02490	.02193	.01592	.01109	.00768	.00536	.00384	.00282	.00160	.00099	.00065
5	.01942	.01938				.01835			.01573	.01249	.00949	.00708	.00527	.00394	.00298	.00179	.00113	.00075
6	.01361					.01307			.01168	.00983	.00795	.00628	.00492	.00384	.00299	.00188	.00124	.00084
7	.01005					.00976			.00894	.00784	.00661	.00548	.00445	.00360	.00291	.00193	.00130	.00091
8	.00772					.00755			.00703	.00635	.00554	.00472	.00398	.00332	.00276	.00189	.00134	.00094
9	.00612					.00600			.00566	.00520	.00466	.00409	.00353	.00301	.00256	.00184	.00133	.00096
10								.00477	.00465	.00438	.00397	.00352	.00326	.00273	.00241			

Table 3

Function "H"

Depth z in radii	Offset in radii 0	0.2	0.4	0.6	0.8	1	1.2	1.5	2	3	4	5	6	7	8	10	12	15
0	2.0	1.97957	1.91751	1.80275	1.62553	1.27319	.93676	.71185	.51671	.33515	.25200	.20045	.16626	.14315	.12576	.09918	.08346	.07023
0.1	1.80998	1.79818	1.72444	1.61961	1.44711	1.18107	.92670	.70888	.51627	.33794	.25184	.20081						
0.2	1.63961	1.62065	1.56242	1.46001	1.30614	1.09996	.90098	.70074	.51382	.33726	.25162	.20072	.16688	.14268	.12512			
0.3	1.48806	1.47344	1.40979	1.32442	1.19210	1.02740	.86726	.68823	.50966	.33638	.25124							
0.4	1.35407	1.33602	1.28963	1.20822	1.09555	.96202	.83042	.67238	.50412									
0.5	1.23607	1.22176	1.17594	1.10830	1.01312	.90298	.79308	.65429	.49728	.33293	.24996	.19982	.16668	.14273	.12493	.09996	.08295	.07123
0.6	1.13238	1.11998	1.08350	1.02154	.94120	.84917	.75653	.63469										
0.7	1.04131	1.03037	.99794	.91049	.87742	.80030	.72143	.61442	.48061									
0.8	.96125	.95175	.92386	.87928	.82136	.75571	.68809	.59398										
0.9	.89072	.88251	.85856	.82616	.77950	.71495	.65677	.57361										
1	.82843	.85005	.80465	.76809	.72587	.67769	.62701	.55364	.45122	.31877	.24386	.19673	.16516	.14182	.12394	.09952	.08292	.07104
1.2	.72410	.71882	.70370	.67937	.64814	.61187	.57329	.51552	.43013	.31162	.24070	.19520	.16369	.14099	.12350			
1.5	.60555	.60233	.57246	.57633	.55559	.53138	.50496	.46379	.39872	.29945	.23495	.19053	.16199	.14058	.12281	.09976	.08270	.07064
2	.47214	.47022	.44512	.45656	.44502	.43202	.41702	.39242	.35054	.27740	.22418	.18618	.15846	.13762	.12124	.09792	.08196	.07026
2.5	.38516	.38403	.38098	.37608	.36940	.36155	.35243	.33698	.30913	.25550	.21208	.17898	.15395	.13463	.11928	.09700	.08115	.06980
3	.32457	.32403	.32184	.31887	.31464	.30969	.30381	.29364	.27453	.23487	.19977	.17154	.14919	.13119	.11694	.09558	.08061	.06897
4	.24620	.24588	.24820	.25128	.24168	.23932	.23668	.23164	.22188	.19908	.17640	.15596	.13564	.12396	.11172	.09300	.07964	.06848
5	.19805	.19785				.19455			.18450	.17080	.15575	.14130	.12785	.11615	.10585	.08915	.07675	.06695
6	.16554					.16326			.15750	.14868	.13842	.12792	.11778	.10836	.09990	.08562	.07452	.06522
7	.14217					.14077			.13699	.13097	.12404	.11620	.10843	.10101	.09387	.08197	.07210	.06377
8	.12448					.12352			.12112	.11680	.11176	.10600	.09976	.09400	.08848	.07800	.06928	.06200
9	.11079					.10989			.10854	.10548	.10161	.09702	.09234	.08754	.08298	.07407	.06678	.05976
10								.09900	.09820	.09510	.09290	.08980	.08300	.08180	.07710			

Table 4. Deflection Factors for $\nu = 0.5$

Depth z in radii	Offset in radii																
	0	0.2	0.4	0.6	0.8	1	1.2	1.5	2	3	4	5	6	7	8	10	12	14
0	1.500	1.485	1.438	1.354	1.219	0.955	0.703	0.534	0.388	0.254	0.189	0.150	0.125	0.107	0.094	0.074	0.063	0.053
0.1	1.493	1.477	1.430	1.344	1.204	0.950	0.709	0.536	0.388	0.254	0.189	0.151	—	—	—	—	—	—
0.2	1.471	1.455	1.405	1.315	1.165	0.940	0.722	0.541	0.390	0.254	0.189	0.151	0.125	0.107	0.094	—	—	—
0.3	1.437	1.420	1.365	1.275	1.128	0.925	0.731	0.549	0.393	0.255	0.190	—	—	—	—	—	—	—
0.4	1.393	1.376	1.323	1.229	1.088	0.908	0.735	0.556	0.397	—	—	—	—	—	—	—	—	—
0.5	1.342	1.324	1.271	1.180	1.048	0.888	0.734	0.562	0.401	0.257	0.191	0.151	0.126	0.108	0.094	0.075	0.062	0.053
0.6	1.286	1.269	1.218	1.130	1.009	0.867	0.729	0.566	—	—	—	—	—	—	—	—	—	—
0.7	1.229	1.212	1.163	1.055	0.971	0.828	0.721	0.568	0.403	—	—	—	—	—	—	—	—	—
0.8	1.172	1.156	1.110	1.034	0.935	0.822	0.711	0.568	—	—	—	—	—	—	—	—	—	—
0.9	1.115	1.101	1.058	0.994	0.906	0.799	0.698	0.566	—	—	—	—	—	—	—	—	—	—
1.0	1.061	1.049	1.009	0.947	0.866	0.776	0.685	0.563	0.415	0.265	0.194	0.153	0.127	0.109	0.094	0.075	0.063	0.054
1.2	0.960	0.949	0.918	0.868	0.803	0.731	0.656	0.552	0.417	0.269	0.196	0.155	0.128	0.109	0.095	—	—	—
1.5	0.832	0.824	0.787	0.765	0.719	0.666	0.610	0.529	0.414	0.273	0.199	0.155	0.129	0.110	0.095	0.076	0.063	0.054
2.0	0.671	0.666	0.638	0.632	0.604	0.572	0.537	0.483	0.393	0.275	0.203	0.159	0.131	0.111	0.096	0.076	0.063	0.054
2.5	0.557	0.554	0.546	0.533	0.516	0.495	0.473	0.436	0.374	0.272	0.205	0.162	0.133	0.113	0.097	0.077	0.063	0.054
3.0	0.474	0.473	0.467	0.459	0.448	0.434	0.419	0.393	0.340	0.265	0.205	0.163	0.135	0.114	0.099	0.078	0.064	0.054
4.0	0.364	0.363	0.361	0.357	0.351	0.344	0.337	0.323	0.298	0.245	0.199	0.163	0.136	0.116	0.101	0.079	0.065	0.055
5.0	0.294	0.294	—	—	—	0.284	—	—	0.256	0.222	0.188	0.159	0.135	0.117	0.102	0.080	0.066	0.056
6.0	0.247	—	—	—	—	0.240	—	—	0.223	0.200	0.175	0.152	0.133	0.116	0.102	0.081	0.067	0.056
7.0	0.212	—	—	—	—	0.208	—	—	0.197	0.181	0.162	0.145	0.128	0.114	0.101	0.082	0.068	0.057
8.0	0.186	—	—	—	—	0.183	—	—	0.175	0.164	0.150	0.136	0.123	0.110	0.099	0.081	0.068	0.058
9.0	0.166	—	—	—	—	0.163	—	—	0.158	0.149	0.139	0.128	0.117	0.107	0.097	0.080	0.068	0.059
10.0	—	—	—	—	—	—	—	0.144	0.143	0.137	0.129	0.120	0.111	0.102	0.094	—	—	—

Table 5. Deflection Factors for $\nu = 0.4$

Depth z in radii	Offset in radii																	
	0	0.2	0.4	0.6	0.8	1	1.2	1.5	2	3	4	5	6	7	8	10	12	14
0	1.660	1.663	1.611	1.517	1.365	1.069	0.787	0.598	0.434	0.284	0.212	0.168	0.140	0.120	0.106	0.083	0.070	0.059
0.1	1.646	1.629	1.576	1.481	1.326	1.052	0.792	0.599	0.435	0.284	0.212	0.169	—	—	—	—	—	—
0.2	1.602	1.585	1.531	1.432	1.274	1.031	0.800	0.603	0.436	0.284	0.212	0.169	0.140	0.120	0.105	—	—	—
0.3	1.549	1.531	1.471	1.376	1.220	1.007	0.804	0.608	0.438	0.285	0.212	—	—	—	—	—	—	—
0.4	1.489	1.471	1.415	1.316	1.169	0.982	0.802	0.613	0.441	—	—	—	—	—	—	—	—	—
0.5	1.425	1.407	1.352	1.256	1.120	0.956	0.796	0.616	0.444	0.287	0.213	0.169	0.141	0.120	0.105	0.084	0.070	0.060
0.6	1.359	1.341	1.289	1.198	1.073	0.928	0.786	0.617	—	—	—	—	—	—	—	—	—	—
0.7	1.293	1.276	1.225	1.112	1.029	0.885	0.774	0.616	0.448	—	—	—	—	—	—	—	—	—
0.8	1.228	1.212	1.165	1.089	0.988	0.873	0.760	0.614	—	—	—	—	—	—	—	—	—	—
0.9	1.165	1.151	1.108	1.043	0.955	0.846	0.744	0.609	—	—	—	—	—	—	—	—	—	—
1.0	1.106	1.117	1.054	0.991	0.910	0.819	0.727	0.603	0.452	0.292	0.215	0.171	0.142	0.121	0.105	0.084	0.070	0.060
1.2	0.995	0.987	0.955	0.905	0.841	0.768	0.693	0.587	0.450	0.294	0.217	0.172	0.142	0.121	0.106	—	—	—
1.5	0.861	0.854	0.814	0.795	0.749	0.696	0.640	0.559	0.442	0.297	0.219	0.172	0.143	0.122	0.106	0.084	0.070	0.060
2.0	0.692	0.688	0.658	0.654	0.626	0.594	0.559	0.505	0.420	0.295	0.221	0.175	0.144	0.123	0.107	0.085	0.070	0.060
2.5	0.574	0.571	0.563	0.550	0.533	0.513	0.490	0.454	0.392	0.290	0.221	0.176	0.146	0.124	0.108	0.086	0.071	0.060
3.0	0.488	0.486	0.481	0.473	0.462	0.449	0.433	0.408	0.363	0.280	0.219	0.176	0.147	0.125	0.108	0.086	0.071	0.060
4.0	0.374	0.373	0.371	0.368	0.362	0.355	0.347	0.334	0.309	0.256	0.210	0.174	0.146	0.126	0.110	0.087	0.072	0.061
5.0	0.302	0.302	—	—	—	0.292	—	—	0.265	0.231	0.197	0.168	0.144	0.125	0.110	0.087	0.072	0.061
6.0	0.253	—	—	—	—	0.247	—	—	0.230	0.207	0.183	0.160	0.140	0.123	0.109	0.088	0.073	0.062
7.0	0.218	—	—	—	—	0.214	—	—	0.203	0.187	0.169	0.151	0.135	0.120	0.107	0.088	0.073	0.062
8.0	0.191	—	—	—	—	0.188	—	—	0.180	0.169	0.156	0.142	0.128	0.116	0.105	0.087	0.073	0.063
9.0	0.170	—	—	—	—	0.168	—	—	0.162	0.154	0.144	0.133	0.122	0.112	0.102	0.085	0.073	0.062
10.0	—	—	—	—	—	—	—	0.148	0.148	0.141	0.134	0.125	0.115	0.107	0.099	—	—	—

Table 6. Deflection Factors for $\nu = 0.3$

Depth z in radii	Offset in radii																	
	0	0.2	0.4	0.6	0.8	1	1.2	1.5	2	3	4	5	6	7	8	10	12	14
0	1.820	1.802	1.745	1.643	1.479	1.159	0.852	0.648	0.473	0.308	0.229	0.182	0.151	0.130	0.114	0.090	0.076	0.064
0.1	1.764	1.746	1.689	1.586	1.419	1.131	0.856	0.649	0.471	0.308	0.229	0.183	—	—	—	—	—	—
0.2	1.701	1.682	1.624	1.520	1.352	1.100	0.860	0.651	0.472	0.308	0.229	0.183	0.152	0.130	0.114	—	—	—
0.3	1.632	1.613	1.549	1.450	1.288	1.069	0.859	0.654	0.473	0.309	0.230	—	—	—	—	—	—	—
0.4	1.559	1.540	1.482	1.379	1.227	1.037	0.853	0.657	0.475	—	—	—	—	—	—	—	—	—
0.5	1.484	1.465	1.408	1.310	1.171	1.005	0.842	0.657	0.477	0.310	0.230	0.183	0.152	0.130	0.114	0.091	0.076	0.065
0.6	1.409	1.391	1.338	1.245	1.119	0.972	0.828	0.656	—	—	—	—	—	—	—	—	—	—
0.7	1.336	1.319	1.267	1.151	1.070	0.926	0.812	0.652	0.479	—	—	—	—	—	—	—	—	—
0.8	1.265	1.249	1.202	1.125	1.024	0.909	0.795	0.647	—	—	—	—	—	—	—	—	—	—
0.9	1.198	1.183	1.140	1.076	0.988	0.879	0.776	0.640	—	—	—	—	—	—	—	—	—	—
1.0	1.135	1.147	1.083	1.020	0.940	0.849	0.757	0.632	0.478	0.313	0.232	0.184	0.153	0.131	0.114	0.091	0.076	0.065
1.2	1.021	1.010	0.978	0.929	0.865	0.792	0.718	0.613	0.473	0.314	0.233	0.185	0.153	0.131	0.114	—	—	—
1.5	0.879	0.871	0.831	0.813	0.768	0.715	0.660	0.579	0.463	0.314	0.234	0.184	0.154	0.132	0.115	0.091	0.076	0.065
2.0	0.704	0.700	0.669	0.666	0.639	0.608	0.574	0.520	0.436	0.310	0.234	0.187	0.155	0.132	0.115	0.092	0.076	0.065
2.5	0.583	0.580	0.572	0.560	0.543	0.523	0.501	0.465	0.404	0.302	0.233	0.187	0.155	0.133	0.115	0.092	0.076	0.065
3.0	0.496	0.494	0.489	0.481	0.470	0.457	0.442	0.417	0.373	0.291	0.229	0.186	0.155	0.133	0.116	0.092	0.076	0.065
4.0	0.379	0.379	0.377	0.374	0.367	0.361	0.353	0.340	0.316	0.264	0.218	0.182	0.154	0.133	0.116	0.093	0.077	0.065
5.0	0.306	0.306	—	—	—	0.296	—	—	0.270	0.237	0.203	0.175	0.151	0.131	0.116	0.093	0.077	0.065
6.0	0.257	—	—	—	—	0.251	—	—	0.234	0.212	0.188	0.165	0.146	0.129	0.114	0.093	0.077	0.066
7.0	0.221	—	—	—	—	0.217	—	—	0.206	0.191	0.173	0.156	0.139	0.125	0.112	0.092	0.077	0.065
8.0	0.194	—	—	—	—	0.191	—	—	0.183	0.172	0.159	0.146	0.132	0.120	0.109	0.091	0.077	0.066
9.0	0.172	—	—	—	—	0.170	—	—	0.165	0.157	0.147	0.136	0.125	0.115	0.105	0.089	0.076	0.066
10.0	—	—	—	—	—	—	—	0.150	0.150	0.143	0.136	0.127	0.118	0.110	0.101	—	—	—

Table 7. Deflection Factors for $\nu = 0.2$

Depth z in radii	Offset in radii																	
	0	0.2	0.4	0.6	0.8	1	1.2	1.5	2	3	4	5	6	7	8	10	12	∞
0	1.920	1.901	1.841	1.734	1.561	1.222	0.899	0.653	0.496	0.325	0.242	0.192	0.160	0.137	0.121	0.095	0.080	0.067
0.1	1.816	1.825	1.766	1.658	1.484	1.185	0.901	0.684	0.497	0.325	0.242	0.193	—	—	—	—	—	—
0.2	1.767	1.747	1.687	1.576	1.405	1.148	0.902	0.685	0.497	0.325	0.242	0.193	0.160	0.137	0.120	—	—	—
0.3	1.635	1.665	1.599	1.497	1.332	1.110	0.897	0.687	0.498	0.325	0.242	—	—	—	—	—	—	—
0.4	1.602	1.562	1.522	1.418	1.265	1.073	0.887	0.687	0.499	—	—	—	—	—	—	—	—	—
0.5	1.518	1.499	1.442	1.343	1.203	1.036	0.873	0.685	0.500	0.326	0.242	0.193	0.161	0.137	0.120	0.096	0.080	0.068
0.6	1.437	1.419	1.365	1.272	1.146	0.999	0.856	0.681	—	—	—	—	—	—	—	—	—	—
0.7	1.358	1.341	1.290	1.172	1.093	0.951	0.836	0.676	0.500	—	—	—	—	—	—	—	—	—
0.8	1.283	1.267	1.220	1.144	1.044	0.930	0.816	0.668	—	—	—	—	—	—	—	—	—	—
0.9	1.213	1.198	1.155	1.092	1.006	0.897	0.795	0.660	—	—	—	—	—	—	—	—	—	—
1.0	1.147	1.161	1.097	1.034	0.954	0.865	0.774	0.650	0.495	0.327	0.243	0.194	0.161	0.138	0.120	0.096	0.080	0.068
1.2	1.029	1.018	0.987	0.939	0.876	0.805	0.731	0.627	0.489	0.327	0.244	0.194	0.161	0.138	0.120	—	—	—
1.5	0.884	0.876	0.835	0.820	0.715	0.724	0.670	0.590	0.475	0.326	0.244	0.193	0.161	0.139	0.120	0.096	0.080	0.068
2.0	0.701	0.702	0.671	0.670	0.643	0.613	0.560	0.527	0.444	0.320	0.243	0.195	0.162	0.138	0.121	0.096	0.080	0.068
2.5	0.554	0.582	0.574	0.562	0.546	0.526	0.505	0.470	0.410	0.310	0.240	0.194	0.162	0.138	0.121	0.097	0.081	0.069
3.0	0.496	0.495	0.490	0.482	0.472	0.459	0.444	0.420	0.377	0.297	0.236	0.192	0.161	0.138	0.121	0.097	0.080	0.069
4.0	0.390	0.389	0.388	0.386	0.368	0.362	0.354	0.342	0.318	0.268	0.223	0.187	0.159	0.137	0.121	0.097	0.080	0.069
5.0	0.307	0.306	—	—	—	0.297	—	—	0.272	0.239	0.206	0.178	0.154	0.135	0.119	0.096	0.080	0.069
6.0	0.257	—	—	—	—	0.251	—	—	0.235	0.214	0.190	0.168	0.148	0.132	0.117	0.096	0.080	0.069
7.0	0.221	—	—	—	—	0.217	—	—	0.207	0.192	0.175	0.158	0.141	0.127	0.115	0.095	0.080	0.069
8.0	0.194	—	—	—	—	0.191	—	—	0.184	0.173	0.160	0.147	0.134	0.122	0.111	0.093	0.079	0.069
9.0	0.172	—	—	—	—	0.170	—	—	0.165	0.157	0.148	0.137	0.127	0.117	0.107	0.091	0.078	0.068
10.0	—	—	—	—	—	—	—	0.151	0.150	0.144	0.137	0.128	0.119	0.111	0.103	—	—	—

Table 8

Maximum Deflection Factors for Single Wheels

Depth z in radii	Maximum Deflection Factors			
	$\nu = 0.5$	$\nu = 0.4$	$\nu = 0.3$	$\nu = 0.2$
0.0	1.500	1.680	1.820	1.920
0.1	1.493	1.646	1.764	1.846
0.2	1.471	1.602	1.701	1.767
0.3	1.437	1.549	1.632	1.685
0.4	1.393	1.489	1.559	1.602
0.5	1.342	1.425	1.484	1.518
0.6	1.286	1.359	1.409	1.437
0.7	1.229	1.293	1.336	1.358
0.8	1.171	1.228	1.265	1.283
0.9	1.115	1.165	1.198	1.213
1.0	1.061	1.106	1.135	1.147
1.2	0.960	0.998	1.021	1.029
1.5	0.832	0.861	0.879	0.884
2.0	0.671	0.692	0.704	0.707
2.5	0.557	0.574	0.583	0.584
3.0	0.474	0.488	0.496	0.496
4.0	0.364	0.374	0.379	0.380
5.0	0.294	0.302	0.306	0.307
6.0	0.247	0.253	0.257	0.257
7.0	0.212	0.218	0.221	0.221
8.0	0.186	0.191	0.194	0.194
9.0	0.166	0.170	0.172	0.172

Table 9

Maximum Deflection Factors for Single Wheel; $\nu = 0.4$

Depth		F_e	Depth		F_e
radii	in.		radii	in.	
0.0	0.00	1.680	3.0	20.73	0.488
0.1	0.69	1.646	4.0	27.64	0.374
0.2	1.38	1.602	5.0	34.55	0.302
0.5	3.46	1.425	6.0	41.46	0.253
1.0	6.91	1.106	7.0	48.37	0.218
1.5	10.37	0.861	8.0	55.28	0.191
2.0	13.82	0.692	9.0	62.19	0.170

Table 10

Deflection Factors Beneath One Tire for Multiple Wheels

Depth		Single-Wheel Deflection Factors, F_e		Multiple-Wheel Deflection Factors F_M
radii (1)	in. (2)	0.0-radii offset (3)	3.76-radii offset (4)	0.0-radii offset (5) = (3) + (4)
0.0	0.00	1.680	0.229	1.909
0.1	0.69	1.646	0.229	1.875
0.2	1.38	1.602	0.229	1.831
0.5	3.46	1.425	0.231	1.656
1.0	6.91	1.106	0.233	1.339
1.5	10.37	0.861	0.238	1.099
2.0	13.82	0.692	0.239	0.931
3.0	20.73	0.488	0.234	0.722
4.0	27.64	0.374	0.221	0.595
5.0	34.55	0.302	0.205	0.507
6.0	41.46	0.253	0.189	0.442
7.0	48.37	0.218	0.173	0.391
8.0	55.28	0.191	0.159	0.350
9.0	62.19	0.170	0.146	0.316

Table 11

Multiple-Wheel Deflection Factors Under Center of Gravity

Depth		Deflection Factors	
		Single Wheel, F_e	Multiple Wheel, F_M
radii (1)	in. (2)	1.88-radii offset (3)	Center of assembly (4) = 2 × (3)
0.0	0.00	0.510	1.020
0.1	0.69	0.509	1.018
0.2	1.38	0.507	1.014
0.5	3.46	0.505	1.010
1.0	6.91	0.496	0.992
1.5	10.37	0.472	0.944
2.0	13.82	0.441	0.882
3.0	20.73	0.373	0.746
4.0	27.64	0.315	0.630
5.0	34.55	0.268	0.536
6.0	41.46	0.232	0.464
7.0	48.37	0.204	0.408
8.0	55.28	0.181	0.362
9.0	62.19	0.163	0.326

Table 12

ESWL Calculations

Depth in. (1)	Maximum Deflection Factors for Multiple Wheels F_M (2)	Single-Wheel Deflection Factor F_e (3)	$\frac{F_M}{F_e}$ (4)	Load per Tire P lb (5)	ESWL, P_e lb (6) = (5) × (4)	ESWL, P_e percent assembly load (7) = [(6) ÷ 2 × (5)] × 100
0.00	1.909	1.680	1.136	13,500	15,336	56.8
0.69	1.875	1.646	1.139		15,376	56.9
1.38	1.831	1.602	1.143		15,430	57.1
3.46	1.656	1.425	1.162		15,687	58.1
6.91	1.339	1.106	1.211		16,348	60.5
10.37	1.099	0.861	1.276		17,226	63.8
13.82	0.935	0.692	1.351		18,238	67.5
20.73	0.750	0.488	1.573		20,749	76.9
27.64	0.630	0.374	1.684		22,734	84.2
34.55	0.536	0.302	1.775		23,962	88.7
41.46	0.464	0.253	1.834		24,759	91.7
48.37	0.408	0.218	1.872		25,272	93.6
55.28	0.362	0.191	1.895		25,582	94.7
62.19	0.326	0.170	1.918		25,893	95.9

Table 13

Ordinates of GND Curve

z	f(z)	$x = \sigma_x z$ in.	$f(x) = \frac{1}{\sigma_x} f(z)$
0.00	0.3989	0.0	0.0131
0.20	0.3910	6.1	0.0128
0.50	0.3521	15.2	0.0116
1.00	0.2420	30.4	0.0080
1.50	0.1295	45.6	0.0042
2.00	0.0540	60.9	0.0018

Table 14

Maximum Deflection Factors for Single Wheel; $\nu = 0.5$

Depth		F_e	Depth		F_e
radii	in.		radii	in.	
0.0	0.00	1.500	3.0	24.42	0.474
0.1	0.81	1.493	4.0	32.56	0.364
0.2	1.63	1.471	5.0	40.70	0.294
0.5	4.07	1.342	6.0	48.84	0.247
1.0	8.14	1.061	7.0	56.98	0.212
1.5	12.21	0.832	8.0	65.12	0.186
2.0	16.28	0.671	9.0	73.26	0.166

Table 15

Deflection Factors Beneath One Wheel for Twin-Tandem Gear

Depth		Deflection Factors at Indicated Offset for Single Wheel				Multiple-Wheel Deflection Factors Below One Wheel (Point 1)
radii	in.	0.00 radii	3.99 radii	5.90 radii	7.12 radii	
0.0	0.00	1.500	0.190	0.128	0.105	1.923
0.1	0.81	1.493	0.190	0.128	0.105	1.916
0.2	1.63	1.471	0.190	0.128	0.105	1.894
0.5	4.07	1.342	0.192	0.129	0.106	1.769
1.0	8.14	1.061	0.195	0.130	0.107	1.493
1.5	12.21	0.832	0.200	0.132	0.108	1.272
2.0	16.28	0.671	0.204	0.134	0.109	1.118
3.0	24.42	0.474	0.206	0.138	0.112	0.930
4.0	32.56	0.364	0.199	0.139	0.114	0.816
5.0	40.70	0.294	0.188	0.137	0.115	0.734
6.0	48.84	0.247	0.175	0.135	0.114	0.671
7.0	56.98	0.212	0.162	0.130	0.112	0.616
8.0	65.12	0.186	0.150	0.124	0.109	0.569
9.0	73.26	0.166	0.139	0.118	0.106	0.529

Table 16

Deflection Factors at Centroid of Assembly for Twin-Tandem Gear

Depth		Single-Wheel Deflection Factors at 3.56-Radii Offset	Multiple-Wheel Deflection Factors at Centroid of Assembly (Point 2 of Figure 22)
Radii	in.		
0.0	0.00	0.218	0.872
0.1	0.81	0.218	0.872
0.2	1.63	0.218	0.872
0.5	4.07	0.220	0.880
1.0	8.14	0.225	0.900
1.5	12.21	0.232	0.928
2.0	16.28	0.235	0.940
3.0	24.42	0.231	0.924
4.0	32.56	0.219	0.876
5.0	40.70	0.203	0.812
6.0	48.84	0.186	0.744
7.0	56.98	0.170	0.680
8.0	65.12	0.156	0.624
9.0	73.26	0.143	0.572

Table 17

Deflection Factors at Intermediate Point for Twin-Tandem Gear

Depth		Single-Wheel Deflection Factors at Indicated Offset				Multiple-Wheel Deflection Factors at Point 3
radii	in.	1.72 radii	2.58 radii	5.28 radii	5.61 radii	
0.0	0.00	0.547	0.310	0.143	0.135	1.135
0.1	0.81	0.545	0.310	0.144	0.136	1.135
0.2	1.63	0.544	0.311	0.144	0.136	1.135
0.5	4.07	0.537	0.317	0.144	0.136	1.134
1.0	8.14	0.517	0.328	0.146	0.137	1.128
1.5	12.21	0.485	0.332	0.148	0.139	1.104
2.0	16.28	0.447	0.327	0.151	0.142	1.067
3.0	24.42	0.372	0.300	0.155	0.146	0.973
4.0	32.56	0.311	0.267	0.155	0.147	0.880
5.0	40.70	0.264	0.236	0.152	0.144	0.796
6.0	48.84	0.228	0.210	0.147	0.140	0.725
7.0	56.98	0.200	0.188	0.140	0.135	0.663
8.0	65.12	0.177	0.169	0.132	0.128	0.606
9.0	73.26	0.159	0.153	0.125	0.121	0.558

Table 18

Calculation of ESWL as a Percent of the Assembly Load

Depth in.	Maximum Multiple-Wheel Deflection Factor	Single-Wheel Deflection Factor	Ratio of Multiple-Wheel to Single-Wheel Deflection Factors	Load on One Wheel of Gear lb	ESWL lb	ESWL percent gear load
0.00	1.923	1.500	1.282	36,000	46,152	32.1
0.81	1.916	1.493	1.283		46,188	32.1
1.63	1.894	1.471	1.288		46,368	32.2
4.07	1.769	1.342	1.318		47,448	33.0
8.14	1.493	1.061	1.407		50,652	35.2
12.21	1.272	0.832	1.529		55,044	38.2
16.28	1.120	0.671	1.669		60,084	41.7
24.42	0.980	0.474	2.068		74,448	51.7
32.56	0.880	0.364	2.418		87,048	60.5
40.70	0.812	0.294	2.762		99,432	69.1
48.84	0.744	0.247	3.012		108,432	75.3
56.98	0.680	0.212	3.208		115,488	80.2
65.12	0.624	0.186	3.355		120,780	83.9
73.26	0.572	0.166	3.446		124,056	86.2

Table 19

Thickness/CBR Requirements for 10,000 Passes

Assumed Thickness in. ($t_{10,000}$)	Load Repetition Factor (α)	Standard Thickness in. (T)	$\frac{T}{\sqrt{A_c}}$	$\frac{CBR}{p_e}$	ESWL lb	p_e	CBR
3	0.798	3.79	0.263	0.416	46,368	222.92	92.73
5		6.32	0.438	0.259	47,808	229.85	59.53
10		12.64	0.877	0.113	52,128	250.62	28.32
15		18.96	1.315	0.061	58,176	279.69	17.06
20		25.28	1.753	0.0361	65,952	317.08	11.45
25		31.61	2.192	0.024	74,880	360.00	8.64
30		37.93	2.630	0.0171	83,232	400.15	6.84
40		50.57	3.507	0.0098	98,496	473.54	4.66
50		63.21	4.383	0.0063	110,592	531.69	3.35
60		75.85	5.260	0.0044	117,648	565.62	2.49
70		88.50	6.137	0.0032	122,976	591.23	1.92

Table 20

Thickness/CBR Requirements for 50,000 Passes

Assumed Thickness in. ($t_{50,000}$)	Load Repetition Factor (α)	Standard Thickness in. (T)	$\frac{T}{\sqrt{A_c}}$	$\frac{CBR}{p_e}$	ESWL lb	p_e	CBR
3	0.87	3.44	0.239	0.441	46,368	222.92	98.30
5		5.75	0.399	0.283	47,808	229.85	65.04
10		11.49	0.797	0.129	52,128	250.62	32.33
15		17.24	1.196	0.0722	58,176	279.69	20.19
20		22.99	1.594	0.043	65,952	317.08	13.63
25		28.74	1.993	0.0285	74,880	360.00	10.26
30		34.48	2.391	0.0204	83,232	400.15	8.16
40		45.98	3.188	0.0118	98,496	473.54	5.56
50		57.47	3.985	0.0076	110,592	531.69	4.05
60		68.97	4.783	0.0053	117,648	565.62	3.00
70		80.46	5.580	0.0040	122,976	591.23	2.36

Table 21

Thickness/CBR Requirements for 100,000 Passes

Assumed Thickness in. ($t_{100,000}$)	Load Repetition Factor (α)	Standard Thickness in. (T)	$\frac{T}{\sqrt{A_c}}$	$\frac{CBR}{P_e}$	ESWL lb	P_e	CBR
3	0.90	3.33	0.231	0.445	46,368	222.92	99.2
5	↓	5.56	0.385	0.290	47,808	229.85	66.66
10		11.11	0.771	0.135	52,128	250.62	33.83
15		16.66	1.156	0.076	58,176	279.69	21.26
20		22.22	1.541	0.0455	65,952	317.08	14.43
25		27.78	1.926	0.0304	74,880	360.00	10.94
30		33.33	2.312	0.0219	83,232	400.15	8.76
40		44.44	3.082	0.0126	98,496	473.54	5.97
50		55.56	3.853	0.0082	110,592	531.69	4.33
60		66.67	4.623	0.0057	117,648	565.62	3.22
70		77.78	5.394	0.0042	122,976	591.23	2.50

APPENDIX A: COMPUTER DETERMINATION OF CBR/THICKNESS REQUIREMENTS

The procedure for calculating CBR/thickness design curves has been computerized with the exception of the pass-per-coverage ratios. This appendix presents an input guide, an input file, a problem output, and a program listing for this procedure. The problem output is for the C-141A aircraft as presented in the example in Part V of the main text. The basic data for the problem are:

Aircraft gross weight	= 320,000 lb
Tire contact area	= 208 sq in.
Tire pressure	= 173 psi
Number of wheels under consideration	= 4
Tire spacing	= 32.5 in. by 48 in. (Figure A1)

Other required data are:

Pass levels = 1-7 pass levels as selected. Three pass levels of 10,000, 50,000, and 100,000 were selected for this example.

Alpha values = 1-7 alpha values corresponding to the selected pass levels are obtained from Figure 14 of the main text. Alpha values for this example are 0.798, 0.87, and 0.90.

Radii = The radius of the tire contact area, assuming the area to be a circle. For this example,

$$r = \sqrt{\frac{A_c}{\pi}} = \sqrt{\frac{208}{3.14}} = 8.13 \text{ in.}$$

Grid location and dimensions = The grid is used in the search for the position of maximum deflection for ESWL calculations. Location of the grid may be a trial-and-error procedure for a particular gear, although, with experience, this location can be determined by good engineering judgment. The values of GX and GY represent the X-Y origin of the grid, DGX and DGY the distance between grid lines, and XK and YK the number of grid lines in each direction. The grid used in the sample problem is shown in Figure A1. Normally, the dimensions between grid lines should be in the order of 1/2 radii.

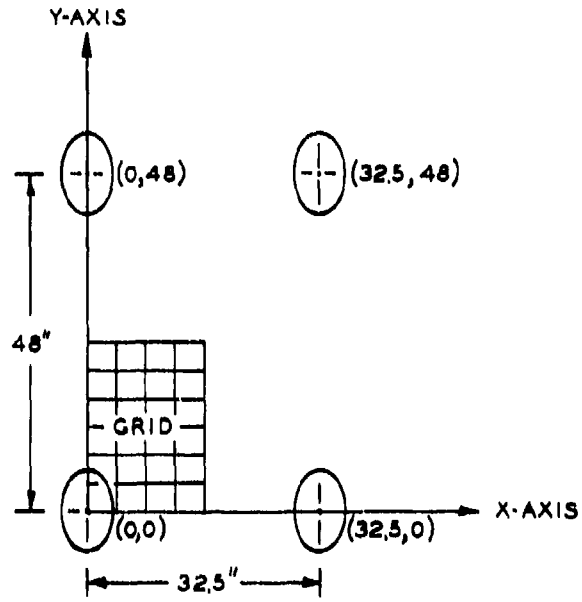

a. WHEEL CONFIGURATION, COORDINATES & GRID LOCATION

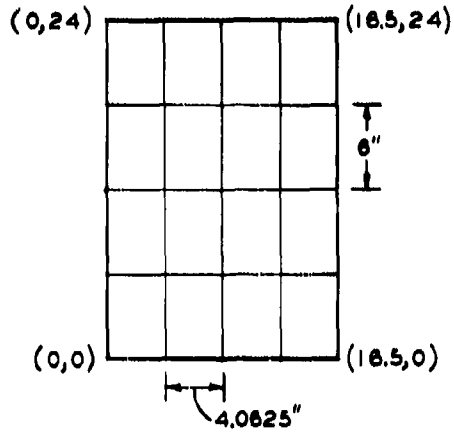

X-DATA	Y-DATA
GX = 0.	GY = 0.
DGX = 4.0625	DGY = 6.
XK = 5.	YK = 5.

b. GRID DIMENSIONS & COORDINATES

Figure A1. C-141A gear and grid for ESWL determinations

Depth for solution = Maximum of 8 and minimum of 2 depths. Input by the number of depths (ZK) and increment (DZ) between depths.

Input Guide

Read Number of Wheels.

Line 100 NW

Read in X-Coordinates.

Line 110 X(i), i = 1, NW

Read in Y-Coordinates.

Line 120 Y(i), i = 1, NW

Note: If NW > 8, then 8 coordinates are the maximum allowed on one data line.

Read Grid Displacement, Increment, and Size for X Axis, then Y Axis.

Line 150 GX, DGX, XK, GY, DGY, YK

Read Number of Depths and Depth Increment.

Line 160 ZK, DZ

Read Number of Maximum Ordered Displacements per Depth.

Line 170 KKZ

Read Number of Sets of Pressures, Radii, and Passes.

Line 180 IPR

Read Equivalent Single-Wheel Radius and Pressure.

Line 190 RESW, PESW

Read Number of Pass Levels and Alpha Values.

Line 200 NAL

Read Passes.

Line 210 NCC(i), i = 1, NAL

Read Alpha Values.

Line 220 B(i), i = 1, NAL

Read Contact Area.

Line 230 CAREA

If another problem desired, return to first input, line 100, and repeat steps through line 230. Begin next problem with a line number greater than 230. The program has no restrictions as to how many problems may be attempted in one run.

Input File

```
 LIST DFILE

100 4
110 0. 32.5 32.5 0.
120 0. 0. 48. 48.
150 0. 4.0625 5. 0. 6. 5.
160 8. 2.
170 2
180 1
190 8.13 173.
200 3
210 10000 50000 100000
220 0.798 0.87 0.9
230 208.

READY

•
```

Program Output

```
RUN CSTAR

        GROUND FLOTATION DESIGN PROGRAM RESULTS


=     C-141A      AIRCRAFT      DESIGN
NUMBER OF WHEELS (MAXIMUM 32)
      4
X COORDINATES OF WHEELS
   0.      32.50    32.50     0.
Y COORDINATES OF WHEELS
   0.       0.      48.00    48.00
LOC. OF GRD.GRD INCPT .NO. OF LINS(MAX=10)
   0.       4.06     5.00     0.       6.00     5.00
NUMBER OF DEP. (MAX 08) AND DEP. INCREMENT
   8.00     2.00
DESIRED NO. OF OPN. MAX. DISPLCMTS PERDEP. (MAX.06)
      2
NO. OF SETS OF PRESS., RAD., AND COV.TO FOLLOW
      1
REFERENCE RADIUS AND PRESSURE
   8.13  173.00
PRESSURES
 173.00  173.00  173.00  173.00
RADII
   8.13     8.13     8.13     8.13
PASSES
    10000       50000      100000
ALPHA VALUES MAX(7)
    0.798       0.870       0.900
CONTACT APER
   208.00
```

DEPTH INS.	DEF. FACTOR	X-CRD. INS.	Y-CRD. INS.	DEPTH INS.	DEF. FACTOR	X-CRD. INS.	Y-CRD. INS.
0.	1.922	0.	0.	8.0	1.499	0.	0.
	1.855	4.06	0.		1.451	4.06	0.
2.0	1.879	0.	0.	10.0	1.380	0.	0.
	1.804	4.06	0.		1.351	4.06	0.
4.0	1.770	0.	0.	12.0	1.279	0.	0.
	1.691	4.06	0.		1.266	4.06	0.
6.0	1.634	0.	0.	14.0	1.195	0.	0.
	1.566	4.06	0.		1.193	4.06	0.

EIWL POUNDS	CBR PASSES 10000	CBR PASSES 50000	CBR PASSES 100000	-T- DEPTH IN.
46031.	294.33	294.33	294.33	0.
46346.	125.95	133.17	135.85	2.00
47246.	71.71	77.78	80.36	4.00
48626.	49.07	53.98	55.84	6.00
50371.	37.19	40.71	42.61	8.00
52386.	29.91	32.23	33.66	10.00
54606.	23.20	26.33	27.80	12.00
56972.	18.99	21.88	23.06	14.00

```
        GROUND FLOTATION DESIGN PROGRAM RESULTS

    END     OF     PROBLEM
```

PROGRAM LISTING

```
70X2T 01  02-21-77   11.186

10ñC      *********      1 MAR 69
11ñC      WES MOD        41-G2-HO-144
12ñC      PROG.  41-Z0-001      GROUND FLOTATION DESIGN *** BOEING AIRCRAFT
13ñC      DOCUMENT  D6-40888TN     TRANSPORT DIVISION, BOX 709, RENTON, WASH;
14ñC
15ñC      NOTE: TO THE ORIGINAL BOEING PROGRAM THE PAVEMENT DESIGN
16ñC      DIVISION , S&PL, WES, HAS MADE SEVERAL CHANGES, THE THICKNESS
17ñC      SOLUTION WAS REPLACED WITH AN INTERPOLATION SCHEME, THE
18ñC      THICKNESS IS NOW DERIVED FROM CBR/P VS, T/SQR(A) CURVE,
19ñC      THE OLD F(PERCENT DESIGN THICKNESS) HAS BEEN REPLACED
20ñC      WITH AN ALPHA VALUE. THE TERM COVERAGES IS REPLACED WITH
21ñC      PASS LEVELS.
22ñC
23ñC      THIS PROGRAM 'CHANG4' IS IDENTICAL TO 'CHANG2'
24ñC      WITH ONE EXCEPTION, AN OPTION IS AVAILABLE TO RUN 1-7
25ñC      PASS LEVELS.
26ñC
27ñC
28ñC
29ñC
30ñC      32              NW   NUMBER OF WHEELS
31ñC      32                        X(NW)      X COORDINATE     IN,  IN,
32ñC      32                        Y(NW)      Y COORDINATE     IN,  IN,
33ñC      32                        RAD(NW)    RADIUS           IN,  IN,
34ñC      32                        RAD2(NW)   RADIUS SQUARED        IN,
35ñC      32                        PR(NW)     PRESSURE              PSI,
36ñC      GX    X COORD OF GRID(DISPLC)              DGX   DELTA X
37ñC      GX    Y COORD OF GRID(DISPLC)              DGY   DELTA Y
38ñC      XK=KX  NUMBER GRID LINKS (SIZE)
39ñC      YK=KY  NUMBER GRID LINKS (SIZE
40ñC      ZK=KZ  NUMBER OF DEPTHS
41ñC      10*               PHI  ANGLE USED IN INTEGRATION
42ñC      10*               CS        COSINE OF PHI
43ñC      10*               SN2       SQ OF SINE OF PHI
44ñC      10,10,8           S(I,J,K)  DISPLACEMENT
45ñC      6                 KKZ   NUMBER OF MAX, ORDERED DISPLACEMENTS/DEPTH
46ñC      IPR   NUMBER SETS OF PRESS.,RADII, & COVERAGES /PROB
47ñC      5                 C     ITH COVERAGE VALUE
48ñC      8                 Z     DEPTH OF ITH WHEEL
49ñC      8                 Z2    Z(I) SQUARED
50ñC
51ñC      RUNNING TIME (MINUTES) = NW * KX * KY * KZ / 80
52ñC
53ñ       COMMON X(32),Y(32),RAD(32),RAD2(32),PR(32)
54ñ       COMMON XG(10),YG(10),S(10,10,8)
55ñ       COMMON Z(8),Z2(8),XLOC(8,96),YLOC(8,96),SD(8,96)
56ñ       COMMON C(5),ESWL(8),CBR(8,7)
57ñ       COMMON SN2(10),CS(10)
58ñ       DIMENSION KTITLE(54)
59ñC
60ñC      X(NW), Y(NW), RAD(NW), RAD2(NW), PR(NW)
61ñC
```

```
70327 01  02-21-77   11.186

62nC      XG(XK), YG(YK),  S(XK, YK, ZK)
63nC
64nC      Z(ZK), Z2(ZK), XLOC(ZK, KKZ), YLOC(ZK, KKZ), BD(ZK, KKZ)
65nC
66nC      C(5),   ESWL(ZK),  CBR(ZK, 5)
67nC
68n       DIMENSION B(7),NCC(7)
69n       DIMENSION U(170),V(170),TA(8,7)
70n       DATA U/1.33,1.,.98,.96,.94,.92,.9,.88,.86,.84,.82,.8,.78
71n8,.76,.74,.72,.7,.68,.66,.64,.62,.6,.59,.58,.57,.56,.55,.54,
72n8,.53,.52,.51,.5,.49,.48,.47,.46,.45,.44,.43,.42,.41,.4,.39,
73n8,.38,.37,.36,.35,.34,.33,.32,.31,.3,.29,.28,.27,.26,.25,.24,.23,.22,
74n8,21,.2,.195,.19,.185,.18,.175,.17,.165,.16,.155,.15,.145,.14,.135,
75n8,.13,.125,.12,.115,.11,.105,.1,.098,.096,.094,.092,.09,.088,
76n8,.086,.084,.082,.08,.078,.076,.074,.072,.07,.068,.066,.064,.062,
77n8,.06,.059,.058,.057,.056,.055,.054,.053,.052,.051,.05,.049,.048,
78n8,.047,.046,.045,.044,.043,.042,.041,.04,.039,.038,.037,.036,.034,
79n8,.032,.03,.029,.028,.027,.026,.025,.024,.023,.022,.021,.02,.019,
80n8,.018,.017,.016,.015,.014,.013,.012,.011,.01,.009,.008,.007,.0065,
81n8,.006,.0055,.005,.0045,.004,.0035,.003,.0025,.002,.00175,.0015,
82n8,.00125,.001,.000875,.00075,.000625,.0005/
83n       DATA V/0.,.048,.05,.055,.06,.061,.065,.07,.078,.08,.085,
84n8,.099,.1,.103,.11,.118,.12,.127,.13,.14,.15,.158,.164,.168,.17,
85n8,.178,.18,.185,.19,.194,.2,.205,.21,.218,.22,.23,.24,.242,.25
86n8,.255,.26,.27,.278,.287,.297,.302,.312,.321,.33,.342,.355,.37,
87n8,.38,.3951,.41,.428,.44,.46,.48,.5,.521,.55,.56,.572,.59,.601,
88n8,.62,.63,.65,.67,.69,.708,.728,.742,.765,.785,.815,.84,.87,
89n8,.9,.93,.958,.97,.985,1.,1.02,1.032,1.045,1.065,1.08,1.1,1.115,
90n81.13,1.15,1.178,1.19,1.21,1.23,1.25,1.27,1.29,1.318,1.331,1.34
91n81.359,1.37,1.382,1.4,1.412,1.43,1.445,1.46,1.475,1.495,1.513,
92n81.53,1.55,1.57,1.59,1.612,1.632,1.65,1.670,1.71,1.73,1.76,
93n81.82,1.881,1.95,1.985,2.023,2.063,2.105,2.149,2.197,2.247,2.298,
94n82.358,2.42,2.486,2.557,2.635,2.72,2.813,2.915,3.029,3.157,3.302,
95n83.468,3.66,3.888,4.162,4.321,4.501,4.704,4.938,5.208,5.528,
96n85.913,6.39,7.007,7.837,8.381,9.056,9.924,11.098,11.87,12.82,
97n814.05,15.7/
98n 799   FORMAT(50H
99nC
100C      ***************  INPUT FORMATS
1010 701   FORMAT ( //  9X,  8HGO HARRY  // )
1020 800   FORMAT  (20A4)
1030 801   FORMAT (10F7.2)
1040 802   FORMAT (9I7)
1050 805   FORMAT ( 1H1, 8H TIMING / 20H Ky,KX,Kz,M,KA,TIME   9I7, F7.2/1H1)
106OC      ***************  OUTPUT FORMATS
1070C
1080 900   FORMAT (1H1)
1090 901   FORMAT(10X,40HGROUND FLOTATION DESIGN PROGRAM RESULTS ///)
1100 902   FORMAT (15X,  20A4, / )
1110 903   FORMAT(29HNUMBER OF WHEELS (MAXIMUM 32)  /I8)
1120 904   FORMAT(23HX COORDINATES OF WHEELS/(9F8.2))
1130 905   FORMAT(23HY COORDINATES OF WHEELS/(9F8.2))
```

```
7032T 01  02-21-77   11.186

1140 906   FORMAT('LOC. OF GRD,GRD INCRT ,NO. OF LINS(MAX(10))'
1150&,/,6F8.2)
1160 907   FORMAT('NUMBER OF DEP. (MAX 06) AND DEP. INCREMENT
1170&',/,2F8.2)
1180 908   FORMAT('DESIRED NO. OF ORD. MAX. DISPLCMTS PER
1190&DEP. (MAX.06)',/,I8)
1200 909   FORMAT('NO. OF SETS OF PRESS., RAD., AND COV.
1210&TO FOLLOW',/,I8)
1220 910   FORMAT(29HREFERENCE RADIUS AND PRESSURE/2F8.2)
1230 911   FORMAT(9HPRESSURES/(9F8.2))
1240 912   FORMAT(5HRADII/(9F8.2))
1250 913   FORMAT(6HPASSES/(5I10))
1260 914   FORMAT(4X,'DEPTH',4X,'DEF.',4X,'X-CRD.',3X,'Y-CRD.',
1270&4X,'DEPTH',4X,'DEF.',4X,'X-CRD.',3X,'Y-CRD.',/,
1280&5X,'INS.',3X,'FACTOR',4X,'INS.',5X,'INS.',
1290&8X,'INS.',3X,'FACTOR',4X,'INS.',5X,'INS.')
1300 915   FORMAT(F9.1,F9.3,F9.2,F9.2,F9.1,F9.3,F9.2,F9.2/
1310&(F18.3,F9.2,F9.2,F18.3,F9.2,F9.2))
1320 916   FORMAT(F9.1,F9.3,F9.2,F9.2/(F18.3,F9.2,F9.2))
1330 917   FORMAT (15X,3HCBR,7X,3HCBR,7X,3HCBR,7X,3HCBR,7X,3HCBR,
1340&7X,3H-T=,/,4X,4HESWL,5X,6HPASSES,4X,6HPASSES,4X,6HPASSES,4X,
1350&6HPASSES,4X,6HPASSES,5X,5HDEPTH,/,3X,6HPOUNDS,I10,I10,I10,
1360&I10,I10,6X,3HIN.,/,(F9.0,6F10.2))
1370       PRINT 900
1380 920   FORMAT('ADJ. THEOR. DEFLECTION .... MAX. OFFSET
1390&IS    ',F7.2,6H RADII //)
1400 925   FORMAT(19HALPHA VALUES MAX(7),/,(5F10.3))
1410 926 FORMAT(12HCONTACT AREA,/F10.2)
1420 927   FORMAT(15X,3HCBR,7X,3H-T=,/,4X,4HESWL,5X,6HPASSES,5X,5HDEPTH,
1430&/,3X,6HPOUNDS,I10,6X,3HIN.,/,(F9.0,2F10.2))
1440 928   FORMAT(15X,3HCBR,7X,3HCBR,7X,3H-T=,/,4X,4HESWL,5X,6HPASSES,
1450&4X,6HPASSES,5X,5HDEPTH,/,3X,6HPOUNDS,2I10,6X,3HIN.,/,(F9.0,3F10.2))
1460 929   FORMAT(15X,3HCBR,7X,3HCBR,7X,3HCBR,7X,3H-T=,/,4X,4HESWL,5X,6H
1470&PASSES,4X,6HPASSES,4X,6HPASSES,5X,5HDEPTH,/3X,6HPOUNDS,3I10,6X,3HIN.,
1480&/,(F9.0,4F10.2))
1490 930   FORMAT(15X,3HCBR,7X,3HCBR,7X,3HCBR,7X,3HCBR,7X,3H-T=,/,4X,
1500&4HESWL,5X,6HPASSES,4X,6HPASSES,4X,6HPASSES,4X,6HPASSES,5X,5HDEPTH,
1510&/,3X,6HPOUNDS,4I10,6X,3HIN.,/,(F9.0,5F10.2))
1520 940 FORMAT(V)
1530     CALL ATTACH(1,"PASF4/DFILE",3,0,,)
1540 5000  CONTINUE
1550       PRINT901
1560C      HEAD CURRENT TITLE CARD
1570       READ 799
1580      READ(1,940)LINENO,NW
1590      IF(NW.GT.7)GO TO 69.
1600      READ(1,940)LINENO,(X(I),I=1,NW)
1610      GO TO 692
1620 691 CONTINUE
1630      READ(1,940)LINENO,(X(I),I=1,8)
1640      IF(NW.LT.9)GO TO 350
1650      READ(1,940)LINENO,(X(I),I=9,16)
```

```
7032T 01  02-21-77   11.186

1660       IF(NW.LT.17)GO TO 350
1670       READ(1,940)LINENO,(X(I),I=17,24)
1680       IF(NW.LT.25)GO TO 350
1690       READ(1,940)LINENO,(X(I),I=25,32)
1700 692   READ(1,940)LINENO,(Y(I),I=1,NW)
1710       GO TO 355
1720 350   READ(1,940)LINENO,(Y(I),I=1,8)
1730       IF(NW.LT.9)GO TO 355
1740       READ(1,940)LINENO,(Y(I),I=9,16)
1750       IF(NW.LT.17)GO TO 355
1760       READ(1,940)LINENO,(Y(I),I=17,24)
1770       IF(NW.LT.25)GO TO 355
1780       READ(1,940)LINENO,(Y(I),I=25,32)
1790 355   CONTINUE
1800C       READ IN GRID DISPLACEMENT, INCREMENT AND SIZE FOR X AND Y=AXIS
1810        READ(1,940)LINENO,GX,DGX,XK,GY,DGY,YK
1820        KX=XK
1830        KY=YK
1840C       READ NUMBER OF DEPTHS AND DEPTH INCREMENT
1850        READ(1,940)LINENO,ZK,DZ
1860        KZ=ZK
1870        M=0
1880        KA=KY*KX*KZ*NW
1890        TIME=KA/450.0
1900C       **************
1910C       NUMBER OF MAXIMUM ORDERED DISPLACEMENTS PER DEPTH REQUIRED
1920        READ(1,940)LINENO,KKZ
1930       READ(1,940)LINENO,IPR
1940C
1950        DO4500,PRS=1,IPR
1960C       READ EQUIV.SINGLE WHEEL RADIUS AND PRESS,
1970C       FACTOR IS IN RADII     *** F = FACTOR / RADL
1980        READ(1,940)LINENO,RESW,PESW
1990        RESW=RESW*RESW
2000       DO 360 I=1,NW
2010       PR(I)=PESW
2020 360   RAD(I)=RESW
2030        IF(IPRS.NE.1) GO TO 739
2040C READ NO. OF PASS LEVELS,
2050        READ(1,940)LINENO, NAL
2060C READ PASSES,
2070       READ(1,940)LINENO,(NCC(I),I=1,NAL)
2080C READ ALPHA'S,
2090        READ(1,940)LINENO, (B(I),I=1,NAL)
2100C READ CONTACT AREA,
2110       READ(1,940)LINENO,CAREA
2120 739    CONTINUE
2130        PRINT903,NW
2140        PRINT904,(X(I),I=1,NW)
2150        PRINT905,(Y(I),I=1,NW)
2160        PRINT906,GX,DGX,XK,GY,DGY,YK
2170        PRINT907,ZK,DZ
```

```
70X2T 01   02-21-77   11.186

2180        PRINT908,KKZ
2190        PRINT909,IPR
2200        PRINT910,RESW,PESW
2210        PRINT911,(PR(I),I=1,NW)
2220        PRINT912,(HAD(I),I=1,NW)
2230        PRINT 913,(NCC(I),I=1,NAL)
2240        PRINT 925,(B(I),I=1,NAL)
2250        PRINT 926,CAREA
2260        PI=3.14159265
2270        DPE=3.0/(2.0*PI*RESW*PESW)
2280C       SET-UP OF GRID DEPTHS
2290        Z(1)=0.0
2300        Z2(1)=0.0
2310C
2320        DO25I=2,KZ
2330        Z(I)=Z(I-1)+DZ
2340        Z2(I)=Z(I)*Z(I)
2350 25      CONTINUE
2360C
2370C       PI/40 = .0785398163397448430
2380C       PI/20 = .1570796326794896661
2390C       PI/10 = .3141592653589793323
2400C       PI   =3.1415926535897932338
2410        PID=0.157079633
2420        PHI=-0.0785398163
2430C       SET-UP SIN(PHI),SQ AND COS(PHI)
2440        DO27I=1,10
2450        PHI=PHI+PID
2460        SINE=SIN(PHI)
2470        SN2(I)=SINE*SINE
2480        CS(I)=COS(PHI)
2490 27      CONTINUE
2500C       SET-UP RADII SQUARED
2510        DO28I=1,NW
2520 28      RADP(I)=RAD(I)*RAD(I)
2530C       SET-UP X-COORDS FOR GRID
2540        XG(1)=GX
2550        DO40I=2,KX
2560 40      XG(I)=XG(I-1)+DGX
2570C       SET-UP Y-COORDS FOR GRID
2580        YG(1)=GY
2590        DO42I=2,KY
2600 42      YG(I)=YG(I-1)+DGY
2610C
2620C       ************************************
2630        DO80I=1,KY
2640        YI=YG(I)
2650        DO78J=1,KX
2660        XJ=XG(J)
2670        DO76K=1,KZ
2680        Z2K=Z2(K)
2690        SS=0.0
```

```
7032T 01   02-21-77   11.186

2700        DO74L=1,NW
2710        RAD2L=RAD2(L)
2720        RADL=RAD(L)
2730        PRL=PH(L)
2740        SJIK=0.0
2750        XLG=X(L)-XJ
2760        R2=XLG*XLG
2770        YLG=Y(L)-YI
2780        R2=YLG*YLG+R2
2790        R=SQRT(R2)
2800        IF(R-RADL)68,68,72
2810C
2820C       SUM DISPLACEMENT DUE TO ONE WHEEL RAD, GREATER THEN R
2830 68      DO71M=1,10
2840        SAR=SQHT(RAD2L-R2*SN2(M))
2850        RC=R*CS(M)
2860        ERP=RC+SAR
2870        ERP2=ERP*ERP
2880        ERM=SAR-RC
2890        ERM2=ERM*ERM
2900 71      SJIK=SJIK+(ERP2/SQRT(ERP2+Z2K)+ERM2/SQHT(ERM2+Z2K))*PID
2910        GOTO120
2920C
2930C       SUM DISPLACEMENT DUE TO ONE WHEEL RAD, LESS THAN R
2940 72      DO73M=1,10
2950        SAR=SQRT(R2-RAD2L*SN2(M))
2960        AC=RADL*CS(M)
2970        SPA=AC+SAR
2980        SPA2=SPA*SPA
2990        SSA=SAR-AC
3000        SSA2=SSA*SSA
3010 73      SJIK=SJIK+AC/SAR*(SPA2/SQRT(SPA2+Z2K)-SSA2/SQRT(SSA2+Z2K))*PID
3020C
3030 120     SJIK=SJIK*PRL
3040 502     SS=SS+SJIK
3050 503     CONTINUE
3060 74      CONTINUE
3070        S(J,I,K)=SS
3080 76      CONTINUE
3090 78      CONTINUE
3100 80      CONTINUE
3110C       ******************************
3120C
3130C
3140        DO222IZ=1,KZ
3150        DO222L=1,KK7
3160        EMAX=0.0
3170C
3180        DO220IX=1,KX
3190        DO220IY=1,KY
3200        IF(S(IX,IY,IZ)-EMAX)220,220,210
3210 210     EMAX=S(IX,IY,IZ)
```

```
70X2T 01   02-21-77   11:186

3290        IXM=IX
3250        IYM=IY
3240        XLOC(IZ,L)=XG(IX)
3250        YLOC(IZ,L)=YG(IY)
3260        SD(IZ,L)=S(IX,IY,IZ)
3270 220     CONTINUE
3280        S(IXM,IYM,IZ)=0.0
3290 222     CONTINUE
3300C
3310C       CALCULATE EQUIV. SINGLE WHEEL LOAD
3320        DO250I=1,KZ
3330 250     ESWL(I)=SD(I,1)*SQRT(RESW2+Z2(I))
3340        SRAREA=SQRT(CAREA)
3350        DO 270 I=1,NAL
3360        KS=2
3370        DO 265 J=1,KZ
3380        TA(J,I)=Z(J)/R(I)
3390        V1=TA(J,I)/SRAREA
3400        IF(V1.NE.0.) GO TO 1500
3410        CBR(J,I)=U(1)*(ESWL(J)/CAREA)
3420        GO TO 267
3430 1500    CONTINUE
3440        DO 266 K=KS,170
3450        IF(V(K).GT.V1) GO TO 1490
3460 266     CONTINUE
3470        PRINT 1480
3480 1480 FORMAT(5X,'***** THICKNESS VALUE CONSIDERED EXCEEDS LIM
3490&ITS OF CURVE *****')
3500        GO TO 4500
3510 1490    UL=ALOG10(U(K-1))+((V1-V(K-1))*(ALOG10(U(K-1))-ALOG10(U(K)
3520&))/(V(K)-V(K-1))
3530        U1=10.**UL
3540        CBR(J,I)=U1*(ESWL(J)/CAREA)
3550        KS=K
3560 267     CONTINUE
3570 265     CONTINUE
3580 270     CONTINUE
3590C
3600        DO330IZ=1,KZ
3610        DO330L=1,KKZ
3620 330     SD(IZ,L)=SD(IZ,L)*DPE
3630C
3640C
3650C       ************      PRINT PAGE 2
3660        PRINT900
3670        PRINT 914
3680        KZ2=KZ/2
3690        KZOVR2=KZ2
3700        IF(KZ-KZ2-KZ2)586,585,586
3710 585     IEVEN=1
3720        GOTO587
3730C
```

```
70327 01  02-21-77   11.186
3740 586    KZOVR2=KZOVR2+1
3750        IEVEN=2
3760        PRINT900
3770 587    DO620I=1,KZOVR2
3780        IK=KZOVR2
3790        L=IK+I
3800        IF(I-KZOVR2)600,590,590
3810 590    GOTO(600,610),IEVEN
3820C
3830 600    PRINT915,(Z(K),SD(K,1),XLOC(K,1),YLOC(K,1),K=I,L,KZOVR2),
3840&((SD(K,J),XLOC(K,J),YLOC(K,J),K=I,L,KZOVR2),J=2,KKZ)
3850        GOTO620
3860C
3870 610    PRINT916,Z(IK),(SD(IK,J),XLOC(IK,J),YLOC(IK,J),J=1,KKZ)
3880 620    CONTINUE
3890C       ************    PRINT  PAGE 3
3900C       PRINT900
3910        IF(NAL.EQ.1) PRINT 927,(NCC(I),I=1,NAL),(ESWL(I),(CBR(I,J),
3920&J=1,NAL),Z(I),I=1,KZ)
3930        IF(NAL.EQ.2) PRINT 928,(NCC(I),I=1,NAL),(ESWL(I),(CBR(I,J),
3940&J=1,NAL),Z(I),I=1,KZ)
3950        IF(NAL.EQ.3) PRINT 929,(NCC(I),I=1,NAL),(ESWL(I),(CBR(I,J),
3960&J=1,NAL),Z(I),I=1,KZ)
3970        IF(NAL.EQ.4) PRINT 930,(NCC(I),I=1,NAL),(ESWL(I),(CBR(I,J),
3980&J=1,NAL),Z(I),I=1,KZ)
3990        IF(NAL.EQ.5) PRINT 917,(NCC(I),I=1,NAL),(ESWL(I),(CBR(I,J),J=1,
4000&5),Z(I),I=1,KZ)
4010        IF(NAL.EQ.6) PRINT 917,(NCC(I),I=1,5),(ESWL(I),(CBR(I,J),J
4020&=1,5),Z(I),I=1,KZ)
4030        IF(NAL.EQ.7) PRINT 917,(NCC(I),I=1,5),(ESWL(I),(CBR(I,J),J
4040&=1,5),Z(I),I=1,KZ)
4050        PRINT 900
4060        IF(NAL.EQ.6) PRINT 927,(NCC(I),I=6,NAL),(ESWL(I),(CBR(I,J),
4070&J=6,NAL),Z(I),I=1,KZ)
4080        IF(NAL.EQ.7) PRINT 928,(NCC(I),I=6,NAL),(ESWL(I),(CBR(I,J),
4090&J=6,NAL),Z(I),I=1,KZ)
4100        PRINT900
4110        PRINT 900
4120 4500   CONTINUE
4130        GO TO 5000.
4140        END
4150
```

In accordance with ER 70-2-3, paragraph 6c(1)(b), dated 15 February 1973, a facsimile catalog card in Library of Congress format is reproduced below.

Pereira, A Taboza

Procedures for development of CBR design curves, by A. Taboza Pereira. Vicksburg, U. S. Army Engineer Waterways Experiment Station, 1977.

1 v. (various pagings) illus. 27 cm. (U. S. Waterways Experiment Station. Instruction report S-77-1)

Prepared for Office, Chief of Engineers, U. S. Army, Washington, D. C., under Project 4A762719AT40, Task A2, Work Unit 001.

Supersedes WES Instruction Report 4, dated Nov. 1959.

Includes bibliography.

1. California Bearing Ratio. 2. Flexible pavements. 3. Pavement design. 4. Pavements. I. U. S. Army. Corps of Engineers. (Series: U. S. Waterways Experiment Station, Vicksburg, Miss. Instruction report S-77-1)

TA7.W34i no.S-77-1